# Structures and Energetics of $H_6^+$ Clusters

**Qiang Hao,[†,‡] Andrew C. Simmonett,[‡] Yukio Yamaguchi,[‡] De-Cai Fang,[†] and Henry F. Schaefer III*[,‡]**

*College of Chemistry, Beijing Normal University, Beijing, 100875, China, and Center for Computational Quantum Chemistry, University of Georgia, Athens, Georgia 30602*

*Received: June 24, 2009; Revised Manuscript Received: August 31, 2009*

Theoretical investigations of the equilibrium structures and associated isomerization reactions of the hydrogen clusters $H_6^+$ have been carried out. Three equilibrium structures and three isomerization transition states were located on the electronic doublet and quartet states of the respective potential energy surfaces. The research employed ab initio self-consistent-field (SCF), coupled cluster (CC) with single and double excitations (CCSD), CCSD with perturbative triple excitations (CCSD(T)), and full triple excitations (CCSDT) wave functions and a wide variety of correlation-consistent polarized valence cc-pVXZ and aug-cc-pVXZ (where X = D, T, Q) basis sets. For each structure the geometry, energy, dipole moment, harmonic vibrational frequencies, and infrared intensities are predicted. Complete active space SCF (CASSCF) and multireference configuration interaction (MRCI) wave functions are used to analyze the effect of correlation on physical properties and energetics. Extensive focal point analyses (including CCSDTQ and full CI energies and basis sets up to sextuple zeta) are used to obtain complete basis set (CBS) limit energies. The $H_2^+$-core $H_6^+$ cluster with $D_{2d}$ symmetry is the global minimum, lying 3.9 (4.2) ± 0.1 kcal mol$^{-1}$ below the $H_3^+$-core $H_6^+$ cluster with $C_s$ symmetry, where zero-point vibrational energy (ZPVE) corrected value are shown in parentheses. The barrier of the isomerization reaction between these two structures is 7.4 (5.2) ± 0.1 kcal mol$^{-1}$. The dissociation energies for the $H_2^+$-core $H_6^+$ isomer [$H_6^+$ ($D_{2d}$) → $2H_2 + H_2^+$] and the $H_3^+$-core $H_6^+$ isomer [$H_6^+$ ($C_s$) → $H_3^+ + H_2 + H$] are 57.5 (50.9) ± 0.1 and 12.3 (8.3) ± 0.1 kcal mol$^{-1}$, respectively.

## Introduction

The hydrogen cluster cations are the simplest molecular aggregate systems and have attracted considerable attention from both experimental and theoretical sides over almost a century.[1−25] It is well-known that the $H_n^+$ clusters are easily produced by electron bombardment or radiation-induced ionization of gaseous $H_2$. In 1912, J. J. Thomson[1] discovered $H_3^+$, and later research showed that the triangular $H_3^+$ ion subsequently attracts neutral $H_2$ to form larger odd-membered $H_{2m+1}^+$ cluster cations.[4,5] It has been shown that even-membered $H_{2m+2}^+$ clusters cations[4,6,9,12] are produced in ionized $H_2$ gas, although their yields are generally much smaller than those for the odd-membered $H_{2m+1}^+$ clusters. Kirchner and Bowers[12] found the relative yields of the even-membered $H_{2m+2}^+$ cluster to be $H_6^+ \gg H_8^+ > H_{10}^+ > H_4^+$. The yield of $H_6^+$ was observed to be by far the largest. This important cluster with an $H_2^+$-core (two $H_2$ molecules bound to the central core) has also been investigated by electron spin resonance (ESR) spectroscopy.[19−21]

An early ab initio study[8] predicted that the $H_6^+$ cluster has a $H_3^+$-core type structure with $C_s$ symmetry. However, later studies[10,16] revealed a more favorable $H_2^+$-core $H_6^+$ cluster with $D_{2d}$ symmetry. In 2007, Kumagai, Inagaki, Kariya, Ushida, Shimizu, and Kumada[21] optimized the geometries of these two isomers at the cc-pVTZ MP2 level of theory, refining the energies with cc-pVQZ QCISD(T) single-point computations. Later, Kakizaki, Takayanagi, and Shiga[22] reported a study at the cc-pVTZ CCSD(T) level of theory. More recently, Scheier and co-workers[24] searched the $H_6^+$ potential energy surface and studied six minima at the aug-cc-pVTZ QCISD level of theory. To our knowledge, these three theoretical studies are the highest levels of theory performed to date.

In the present research, the six different $H_6^+$ structures shown in Scheme 1 are systematically studied using a hierarchical series of highly accurate quantum chemical methods. Spectroscopic fingerprints are determined for these six stationary points to aid future experiments. The relationships between these isomers are discussed, both energetically and structurally, as not all of the structures are minima on the potential energy surface.

## Electronic Structure Considerations

The electronic ground state of the $H_2^+$-core $H_6^+$ cluster with $D_{2d}$ symmetry(**1**) in Scheme 1 has been found to be the $^2A_1$ state with electron configuration

$$(1a_1)^2(1b_2)^2(2a_1) \qquad \tilde{X}\ ^2A_1 \tag{1}$$

The five other $H_6^+$ cluster structures in Scheme 1 have the following symmetries and electron configurations:

$H_3^+$-core cluster with $C_s$ symmetry (**2**)

$$(1a')^2(2a')^2(3a') \qquad \tilde{X}\ ^2A' \tag{2}$$

$H_3^+$-core cluster with $D_{3h}$ symmetry (**3**)

$$(1a'_1)^2(1e')^2(2a'_1) \qquad \tilde{X}\ ^4A'_1 \tag{3}$$

$H_2^+$-core cluster with $D_{2h}$ symmetry (**4**)

* Corresponding author, sch@uga.edu.
† Beijing Normal University.
‡ University of Georgia.

10.1021/jp905928u CCC: $40.75 
Published on Web 10/23/2009

$$(1a_g)^2(1b_{2u})^2(2a_g) \qquad \tilde{X}\ ^2A_g \tag{4}$$

$H_3^+$-core cluster with $C_s$ symmetry (**5**)

$$(1a')^2(2a')^2(3a') \qquad \tilde{X}\ ^2A' \tag{5}$$

$H_3^+$-core cluster with $C_{2v}$ symmetry (**6**)

$$(1a_1)^2(2a_1)^2(3a_1) \qquad \tilde{X}\ ^2A_1 \tag{6}$$

As will be discussed in some detail later, structures **1**−**3** are equilibrium geometries (minima), while structures **4**−**6** are found to be transition states (first-order saddle points) for isomerization reactions.

## Theoretical Methods

In this research the correlation-consistent valence polarized basis sets cc-pVXZ and aug-cc-pVXZ (where X = D, T, Q, 5, 6) developed by Dunning and co-workers[26−28] were utilized. Zeroth-order descriptions of stationary points were obtained using restricted Hartree−Fock (RHF) SCF theory for closed-shell singlet molecules, and both restricted open-shell HF (ROHF) and unrestricted HF (UHF) for open-shell molecules. Dynamic correlation effects were included using coupled-cluster (CC)[29−31] methods with single and double excitations (CCSD),[32−35] CCSD with perturbative triple excitations (CCSD(T)),[36−40] and full triple excitations (CCSDT).[41−43] In this text the CC wave functions adopting RHF (ROHF) references are denoted as RCCSD and RCCSD(T), while those with UHF references are designated as UCCSD, UCCSD(T), and UCCSDT. It is important to note that the coupled cluster treatment was fully unrestricted for both ROHF and UHF references.

In order to analyze changes in geometries and physical properties of $H_6^+$ with respect to the level of correlation treatment, full valence five electrons in six molecular orbitals (5e/6MO) complete active space self-consistent-field (CASSCF)[44,45] and internally contracted multireference configuration interaction (MRCI)[46,47] wave functions were constructed at the aug-cc-pVTZ UCCSD(T) optimized geometries. The numbers of configuration state functions (CSFs) for the CASSCF wave functions are 115 (**1**, **2**, and **5**); 40 (**3**), 59 (**4**), and 64 (**6**). The number of CSFs for the internally contracted MRCI wave functions are 93785 for **1**, 175763 for **2** and **5**, 81878 for **3**, 45809 for **4**, and 87882 for **6**. Because of the light masses involved, diagonal Born−Oppenheimer corrections (DBOC)[48] were computed at the aug-cc-pVQZ RHF (UHF) level of theory.

Focal point analyses (FPA)[49−53] using the ROHF, CCSD, CCSD(T), CCSDT, CC with up to full quadruple excitations (CCSDTQ),[54,55] and full CI (FCI)[56] levels of theory have been performed employing the correlation consistent polarized valence family of basis sets of Dunning and co-workers (cc-pVXZ, X = D, T, Q, 5, 6) to obtain energetic values extrapolated to the complete basis set (CBS) limit. Geometries used for the focal point analysis were optimized at the aug-cc-pVQZ RCCSD(T) level of theory. The total energy extrapolation was partitioned in two terms. The first term corresponds to the total SCF energy and was fitted to the functional form[57]

$$E_{SCF}(X) = A + Be^{-CX} \tag{7}$$

where $A$, $B$, and $C$ are fitting parameters from SCF energies, and $X$ is the cardinal number corresponding to the maximum angular momentum of the basis set. The correlation energy was extrapolated using the formula[58]

$$E_{CORR}(X) = E + FX^{-3} \tag{8}$$

where $E$ and $F$ are fitting parameters from correlation energies and $X$ is the cardinal number mentioned above.

The structures of the stationary points were optimized using analytic derivative methods.[35,38,39,59] Dipole moments were determined analytically for all wave functions as first derivatives of the total energy with respect to external electric field. Harmonic vibrational frequencies were computed via finite differences of analytic first derivatives (gradients) for RCCSD and RCCSD(T) wave functions of all structures and UCCSD, UCCSD(T) wave functions of structure **3**. For remaining wave functions harmonic vibrational frequencies and associated infrared (IR) intensities were determined using analytic second derivative methods.[60,61] Electronic structure computations were carried out using the AcesII (Mainz−Austin−Budapest version),[62,63] Molpro,[64] and Psi3[65] quantum chemistry packages.

## Results and Discussion

The representative optimized geometries of the structures **1**−**6** at six levels of theory with four basis sets (cc-pVTZ, aug-cc-pVTZ, cc-pVQZ, aug-cc-pVQZ) are depicted in Figures 1−6. The corresponding total energies and physical properties for the six structures are provided in Tables 1−6. Natural orbital electron occupation numbers for the valence MOs of the CASSCF wave functions (at the aug-cc-pVTZ UCCSD(T) optimized geometries) are displayed in Table 7. The analogous geometries of $H_2^+$, $H_2$, $H_3^+(D_{3h})$, and $H_5^+(C_{2v})$ are given in Figure 7.

**SCHEME 1: Sketches of Six Different $H_6^+$ Structures**

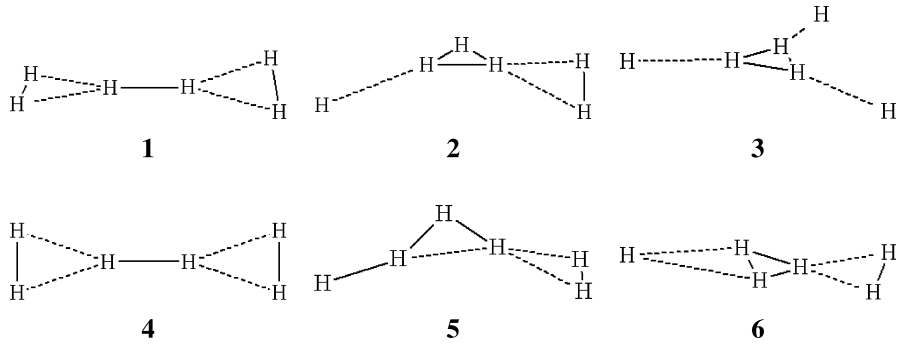

**CASSCF and MRCI Wave Functions.** The reference configuration ($\Phi_1$) and several excited configurations for the full valence (5e/6MO) CASSCF and MRCI wave functions of the six $H_6^+$ structures are presented in the following discussion.

For isomer **1**, the CASSCF wave function is written in terms of its natural orbitals (NOs) as

$$\Psi = 0.986\Phi_1[(1a_1)^2(1b_2)^2(2a_1)] - 0.088\Phi_2[(1a_1)^2(2a_1)(1e)^2] + \ldots \quad (9)$$

The analogous MRCI wave function is described in terms of NOs by

$$\Psi = 0.975\Phi_1[(1a_1)^2(1b_2)^2(2a_1)] - 0.080\Phi_2[(1a_1)^2(2a_1)(1e)^2] + \ldots \quad (10)$$

Only the two CSFs whose CI coefficients are greater in absolute value than 0.05 are shown above. These confirm the predominantly single-reference nature of this isomer. The excited configuration ($\Phi_2$) represents a double excitation from the $1b_2$ MO to the lowest unoccupied MO (LUMO), $(1b_2)^2 \rightarrow (1e)^2$.

For isomer **2**, the CASSCF wave function is written in terms of NOs as

$$\Psi = 0.986\Phi_1[(1a')^2(2a')^2(3a')] - 0.098\Phi_2[(2a')^2(3a')(1a'')^2] - 0.084\Phi_3[(1a')^2(3a')(5a')^2] - 0.082\Phi_4[(1a')^2(3a')(4a')^2] + \ldots \quad (11)$$

The analogous MRCI wave function is described in terms of NOs by

$$\Psi = 0.980\Phi_1[(1a')^2(2a')^2(3a')] - 0.088\Phi_2[(2a')^2(3a')(1a'')^2] - 0.078\Phi_3[(1a')^2(3a')(5a')^2] - 0.076\Phi_4[(1a')^2(3a')(4a')^2] + \ldots \quad (12)$$

There are the only four CSFs with coefficients greater in absolute value than 0.05, and they also confirm the predominantly single-reference nature of this molecule. The three double excitations, $\Phi_2$ $[(1a')^2 \rightarrow (1a'')^2]$, $\Phi_3$ $[(2a')^2 \rightarrow (5a')^2]$, $\Phi_4$ $[(2a')^2 \rightarrow (4a')^2]$, are most important for both the CASSCF and MRCI wave functions.

For the quartet state isomer **3**, the CASSCF wave function is written in terms of NOs as

$$\Psi = 0.992\Phi_1[(1a'_1)^2(1e')^2(2a'_1)] - 0.119\Phi_2[(1e')^2(2a'_1)(2e')^2] + \ldots \quad (13)$$

The analogous MRCI wave function is described in terms of NOs by

$$\Psi = 0.988\Phi_1[(1a'_1)^2(1e')^2(2a'_1)] - 0.110\Phi_2[(1e')^2(2a'_1)(2e')^2] + \ldots \quad (14)$$

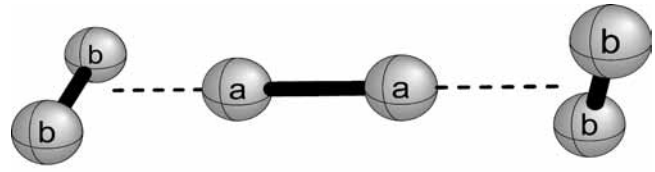


| | | | |
|---|---|---|---|
| ROHF cc-pVTZ | 1.0725 | 1.1810 | 0.7756 |
| ROHF aug-cc-pVTZ | 1.0741 | 1.1811 | 0.7758 |
| ROHF cc-pVQZ | 1.0731 | 1.1818 | 0.7752 |
| ROHF aug-cc-pVQZ | 1.0734 | 1.1818 | 0.7753 |
| UHF cc-pVTZ | 1.0449 | 1.1841 | 0.7780 |
| UHF aug-cc-pVTZ | 1.0461 | 1.1843 | 0.7782 |
| UHF cc-pVQZ | 1.0450 | 1.1850 | 0.7776 |
| UHF aug-cc-pVQZ | 1.0453 | 1.1849 | 0.7777 |
| RCCSD cc-pVTZ | 1.0389 | 1.1596 | 0.7902 |
| RCCSD aug-cc-pVTZ | 1.0406 | 1.1595 | 0.7907 |
| RCCSD cc-pVQZ | 1.0389 | 1.1590 | 0.7898 |
| RCCSD aug-cc-pVQZ | 1.0395 | 1.1590 | 0.7900 |
| UCCSD cc-pVTZ | 1.0385 | 1.1598 | 0.7903 |
| UCCSD aug-cc-pVTZ | 1.0402 | 1.1596 | 0.7908 |
| UCCSD cc-pVQZ | 1.0385 | 1.1592 | 0.7899 |
| UCCSD aug-cc-pVQZ | 1.0391 | 1.1592 | 0.7901 |
| RCCSD(T) cc-pVTZ | 1.0382 | 1.1593 | 0.7908 |
| RCCSD(T) aug-cc-pVTZ | 1.0399 | 1.1591 | 0.7914 |
| RCCSD(T) cc-pVQZ | 1.0382 | 1.1586 | 0.7905 |
| RCCSD(T) aug-cc-pVQZ | 1.0388 | 1.1587 | 0.7906 |
| UCCSD(T) cc-pVTZ | 1.0382 | 1.1593 | 0.7908 |
| UCCSD(T) aug-cc-pVTZ | 1.0399 | 1.1591 | 0.7914 |
| UCCSD(T) cc-pVQZ | 1.0382 | 1.1586 | 0.7905 |
| UCCSD(T) aug-cc-pVQZ | 1.0389 | 1.1586 | 0.7906 |
| UCCSDT cc-pVTZ | 1.0381 | 1.1594 | 0.7910 |
| UCCSDT aug-cc-pVTZ | 1.0399 | 1.1592 | 0.7915 |

**Figure 1.** Predicted geometries for **1**, the $\tilde{X}\ ^2A_1$ equilibrium geometry of the $H_6^+$ molecule in $D_{2d}$ symmetry (isomer **1**). Bond lengths are in angstroms.

These confirm that **3**, like the other minima, does not exhibit excessive multireference character. The most important excited configuration ($\Phi_2$) corresponds to a double excitation from the lowest energy MO to the LUMO, $(1a'_1)^2 \rightarrow (2e')^2$.

For transition state **4**, the CASSCF wave function is written in terms of NOs as

$$\Psi = 0.986\Phi_1[(1a_g)^2(1b_{2u})^2(2a_g)] - 0.088\Phi_2[(1a_g)^2(2a_g)(1b_{3u})^2] + \ldots \quad (15)$$

The analogous MRCI wave function is described in terms of NOs by

$$\Psi = 0.975\Phi_1[(1a_g)^2(1b_{2u})^2(2a_g)] - 0.080\Phi_2[(1a_g)^2(2a_g)(1b_{3u})^2] + \ldots \quad (16)$$

Structure **4** possesses a wave function very similar to that for isomer **1**, and the dominant excited configuration corresponds to a double excitation from the $1b_{2u}$ MO to the LUMO, $(1b_{2u})^2 \rightarrow (1b_{3u})^2$.

For transition state **5**, the CASSCF wave function is written in terms of NOs as

$$\Psi = 0.981\Phi_1[(1a')^2(2a')^2(3a')] - 0.094\Phi_2[(1a')^2(2a')(3a')(4a')] - 0.090\Phi_3[(2a')^2(3a')(1a'')^2] - 0.074\Phi_4[(1a')^2(3a')(4a')^2] - 0.056\Phi_5[(1a')^2(3a')(5a')^2] + \ldots \quad (17)$$

**TABLE 1: Theoretical Predictions of the Total Energy (in Hartree), Harmonic Vibrational Frequencies (in $cm^{-1}$), Infrared (IR) Intensities (in parentheses in km $mol^{-1}$), and Zero-Point Vibrational Energy (ZPVE in kcal $mol^{-1}$) for 1, the $\tilde{X}\ ^2A_1$ Equilibrium Geometry of the $H_6^+$ Molecule in $D_{2d}$ Symmetry (IR intensities for the e modes are doubled)**

| theory | energy | $\omega_1(a_1)$ | $\omega_2(a_1)$ | $\omega_3(a_1)$ | $\omega_4(b_1)$ | $\omega_5(b_2)$ | $\omega_6(b_2)$ | $\omega_7(e)$ | $\omega_8(e)$ | $\omega_9(e)$ | ZPVE |
|---|---|---|---|---|---|---|---|---|---|---|---|
| cc-pVTZ ROHF | −2.935134 | 4056(0.0) | 2024(0.0) | 845(0.0) | 66(0.0) | 3992(941.8) | 594(3019.9) | 1253(25.4) | 883(13.3) | 361(6.6) | 23.69 |
| aug-cc-pVTZ ROHF | −2.935422 | 4052(0.0) | 2015(0.0) | 842(0.0) | 66(0.0) | 3989(937.3) | 587(3010.4) | 1246(29.5) | 875(11.6) | 356(7.2) | 23.60 |
| cc-pVQZ ROHF | −2.936389 | 4051(0.0) | 2014(0.0) | 840(0.0) | 66(0.0) | 3987(941.9) | 575(3011.9) | 1244(27.8) | 875(12.0) | 356(7.3) | 23.57 |
| aug-cc-pVQZ ROHF | −2.936469 | 4051(0.0) | 2012(0.0) | 840(0.0) | 64(0.0) | 3987(940.1) | 574(3010.0) | 1241(29.3) | 872(11.5) | 355(7.3) | 23.54 |
| cc-pVTZ UHF | −2.939068 | 4033(0.0) | 2089(0.0) | 866(0.0) | 68(0.0) | 3944(1197.2) | 711(2919.0) | 1206(18.9) | 805(20.2) | 359(4.3) | 23.52 |
| aug-cc-pVTZ UHF | −2.939333 | 4029(0.0) | 2080(0.0) | 864(0.0) | 67(0.0) | 3940(1188.9) | 705(2909.8) | 1194(23.5) | 797(17.9) | 352(5.3) | 23.41 |
| cc-pVQZ UHF | −2.940323 | 4028(0.0) | 2080(0.0) | 861(0.0) | 68(0.0) | 3939(1196.6) | 697(2911.2) | 1194(21.6) | 796(18.5) | 353(5.1) | 23.38 |
| aug-cc-pVQZ UHF | −2.940399 | 4028(0.0) | 2079(0.0) | 861(0.0) | 66(0.0) | 3938(1193.6) | 696(2909.8) | 1189(23.4) | 793(17.7) | 351(5.4) | 23.35 |
| cc-pVTZ RCCSD | −3.030847 | 3862(0.0) | 2095(0.0) | 905(0.0) | 71(0.0) | 3782(−) | 1010(−) | 1185(−) | 722(−) | 359(−) | 23.24 |
| aug-cc-pVTZ RCCSD | −3.031768 | 3853(0.0) | 2087(0.0) | 904(0.0) | 64(0.0) | 3773(−) | 1006(−) | 1163(−) | 717(−) | 350(−) | 23.08 |
| cc-pVQZ RCCSD | −3.034390 | 3859(0.0) | 2088(0.0) | 903(0.0) | 69(0.0) | 3779(−) | 1002(−) | 1166(−) | 716(−) | 351(−) | 23.11 |
| aug-cc-pVQZ RCCSD | −3.034636 | 3856(0.0) | 2087(0.0) | 902(0.0) | 68(0.0) | 3777(−) | 1002(−) | 1155(−) | 699(−) | 303(−) | 22.88 |
| cc-pVTZ UCCSD | −3.034046 | 3861(0.0) | 2096(0.0) | 905(0.0) | 71(0.0) | 3781(1046.2) | 1012(969.8) | 1184(57.2) | 721(317.6) | 358(435.1) | 23.23 |
| aug-cc-pVTZ UCCSD | −3.034961 | 3852(0.0) | 2088(0.0) | 904(0.0) | 64(0.0) | 3772(1035.9) | 1008(964.6) | 1163(72.1) | 715(298.7) | 350(427.6) | 23.08 |
| cc-pVQZ UCCSD | −3.037598 | 3858(0.0) | 2088(0.0) | 903(0.0) | 69(0.0) | 3778(1044.5) | 1004(963.1) | 1165(68.4) | 714(300.8) | 351(430.9) | 23.10 |
| aug-cc-pVQZ UCCSD | −3.040520 | 3856(0.0) | 2085(0.0) | 903(0.0) | 65(0.0) | 3776(1042.2) | 1002(962.8) | 1156(74.7) | 710(294.2) | 348(428.3) | 23.04 |
| cc-pVTZ RCCSD(T) | −3.037667 | 3854(0.0) | 2098(0.0) | 906(0.0) | 71(0.0) | 3775(−) | 1029(−) | 1181(−) | 710(−) | 357(−) | 23.20 |
| aug-cc-pVTZ RCCSD(T) | −3.038659 | 3845(0.0) | 2090(0.0) | 905(0.0) | 64(0.0) | 3766(−) | 1025(−) | 1159(−) | 705(−) | 349(−) | 23.04 |
| cc-pVQZ RCCSD(T) | −3.041361 | 3851(0.0) | 2091(0.0) | 904(0.0) | 69(0.0) | 3772(−) | 1022(−) | 1161(−) | 704(−) | 350(−) | 23.07 |
| aug-cc-pVQZ RCCSD(T) | −3.041634 | 3849(0.0) | 2087(0.0) | 904(0.0) | 66(0.0) | 3769(−) | 1020(−) | 1151(−) | 699(−) | 347(−) | 23.00 |
| cc-pVTZ UCCSD(T) | −3.037669 | 3854(0.0) | 2098(0.0) | 906(0.0) | 71(0.0) | 3775(1042.8) | 1029(939.5) | 1181(55.1) | 711(326.8) | 357(432.7) | 23.20 |
| aug-cc-pVTZ UCCSD(T) | −3.038661 | 3845(0.0) | 2089(0.0) | 905(0.0) | 65(0.0) | 3766(1032.0) | 1026(934.1) | 1159(69.7) | 706(307.7) | 349(425.4) | 23.05 |
| cc-pVQZ UCCSD(T) | −3.041362 | 3851(0.0) | 2091(0.0) | 904(0.0) | 69(0.0) | 3772(1040.8) | 1022(932.0) | 1161(66.1) | 704(310.1) | 350(428.6) | 23.07 |
| aug-cc-pVQZ UCCSD(T) | −3.041626 | 3849(0.0) | 2087(0.0) | 904(0.0) | 67(0.0) | 3769(1038.3) | 1020(931.7) | 1152(72.4) | 700(303.3) | 347(426.1) | 23.01 |
| cc-pVTZ UCCSDT | −3.037888 | 3852(0.0) | 2098(0.0) | 906(0.0) | 71(0.0) | 3773(1043.7) | 1032(934.3) | 1180(54.5) | 708(329.3) | 357(431.6) | 23.19 |

**TABLE 2: Theoretical Predictions of the Total Energy (in Hartree), Dipole Moment (in Debye), Harmonic Vibrational Frequencies (in $cm^{-1}$), Infrared Intensities (in parentheses in km $mol^{-1}$), and Zero-Point Vibrational Energy (ZPVE in kcal $mol^{-1}$) for 2, the $\tilde{X}\ ^2A'$ Equilibrium Geometry of the $H_6^+$ Molecule in $C_s$ Symmetry**

| theory | energy | $\mu_e$ | $\omega_1(a')$ | $\omega_2(a')$ | $\omega_3(a')$ | $\omega_4(a')$ | $\omega_5(a')$ | $\omega_6(a')$ | $\omega_7(a')$ | $\omega_8(a')$ | $\omega_9(a'')$ | $\omega_{10}(a'')$ | $\omega_{11}(a'')$ | $\omega_{12}(a'')$ | ZPVE |
|---|---|---|---|---|---|---|---|---|---|---|---|---|---|---|---|
| cc-pVTZ ROHF | −2.944440 | 2.087 | 4427(88.3) | 3457(23.3) | 2667(1016.0) | 2550(463.4) | 590(12.9) | 458(302.3) | 376(325.0) | 139(30.8) | 849(0.8) | 674(3.6) | 425(3.3) | 113(4.7) | 23.91 |
| aug-cc-pVTZ ROHF | −2.945099 | 2.137 | 4422(90.5) | 3457(20.9) | 2670(957.9) | 2568(468.3) | 562(21.1) | 446(298.6) | 359(276.5) | 134(31.1) | 831(0.9) | 652(2.2) | 403(3.7) | 120(4.6) | 23.77 |
| cc-pVQZ ROHF | −2.946052 | 2.122 | 4420(89.1) | 3459(21.2) | 2674(987.9) | 2566(462.8) | 572(17.5) | 451(298.5) | 367(292.6) | 137(30.7) | 838(0.8) | 661(2.7) | 414(3.3) | 116(4.5) | 23.84 |
| aug-cc-pVQZ ROHF | −2.946224 | 2.132 | 4419(90.4) | 3460(20.8) | 2673(964.5) | 2569(465.4) | 566(20.4) | 450(302.2) | 361(273.7) | 134(31.1) | 835(0.9) | 656(2.2) | 404(3.6) | 118(4.6) | 23.79 |
| cc-pVTZ UHF | −2.944492 | 2.096 | 4428(88.1) | 3448(21.5) | 2668(1043.9) | 2545(450.5) | 591(12.8) | 458(295.7) | 372(335.2) | 142(30.3) | 847(0.8) | 674(3.5) | 432(3.4) | 113(4.7) | 23.90 |
| aug-cc-pVTZ UHF | −2.945146 | 2.143 | 4423(90.3) | 3449(19.5) | 2671(984.9) | 2563(454.4) | 564(20.9) | 445(292.7) | 355(285.5) | 137(30.7) | 829(0.9) | 652(2.2) | 410(3.7) | 120(4.5) | 23.76 |
| cc-pVQZ UHF | −2.946101 | 2.129 | 4421(88.9) | 3451(19.7) | 2675(1014.5) | 2561(450.1) | 574(17.3) | 450(292.3) | 363(302.1) | 139(30.3) | 835(0.8) | 661(2.6) | 421(3.3) | 116(4.5) | 23.83 |
| aug-cc-pVQZ UHF | −2.946271 | 2.138 | 4419(90.2) | 3451(19.4) | 2674(991.2) | 2564(452.0) | 567(20.2) | 449(295.9) | 357(283.1) | 137(30.6) | 833(0.8) | 656(2.1) | 411(3.7) | 118(4.5) | 23.78 |
| cc-pVTZ RCCSD | −3.028909 | 1.704 | 4221(−) | 3262(−) | 2468(−) | 2201(−) | 733(−) | 536(−) | 414(−) | 196(−) | 936(−) | 747(−) | 550(−) | 122(−) | 23.43 |
| aug-cc-pVTZ RCCSD | −3.030036 | 1.737 | 4211(−) | 3257(−) | 2459(−) | 2222(−) | 704(−) | 525(−) | 398(−) | 184(−) | 912(−) | 732(−) | 531(−) | 125(−) | 23.24 |
| cc-pVQZ RCCSD | −3.034679 | 1.730 | 4217(−) | 3265(−) | 2476(−) | 2222(−) | 713(−) | 535(−) | 413(−) | 189(−) | 922(−) | 741(−) | 538(−) | 122(−) | 23.38 |
| aug-cc-pVQZ RCCSD | −3.034979 | 1.736 | | | | | | | | | | | | | |
| cc-pVTZ UCCSD | −3.030947 | 1.704 | 4221(73.2) | 3261(759.3) | 2468(3177.9) | 2200(222.1) | 733(286.9) | 536(89.2) | 413(181.8) | 196(24.5) | 936(9.0) | 747(18.0) | 550(375.8) | 122(16.5) | 23.43 |
| aug-cc-pVTZ UCCSD | −3.032087 | 1.737 | 4211(73.6) | 3257(762.9) | 2459(3068.1) | 2222(240.3) | 704(305.6) | 525(80.2) | 398(137.6) | 184(22.9) | 912(8.0) | 732(22.6) | 531(383.2) | 125(14.8) | 23.24 |
| cc-pVQZ UCCSD | −3.034680 | 1.731 | 4217(72.8) | 3264(758.6) | 2476(3128.8) | 2222(225.1) | 713(299.4) | 535(83.7) | 413(144.4) | 189(23.7) | 922(8.0) | 741(20.4) | 539(378.5) | 122(15.5) | 23.38 |
| aug-cc-pVQZ UCCSD | −3.035006 | 1.740 | 4213(73.3) | 3264(760.8) | 2472(3082.9) | 2228(233.3) | 707(306.0) | 533(82.6) | 408(129.0) | 184(23.0) | 917(7.7) | 737(23.1) | 529(382.2) | 123(14.8) | 23.32 |
| cc-pVTZ RCCSD(T) | −3.031493 | 1.635 | 4212(−) | 3254(−) | 2444(−) | 2163(−) | 749(−) | 545(−) | 413(−) | 200(−) | 954(−) | 756(−) | 557(−) | 123(−) | 23.40 |
| aug-cc-pVTZ RCCSD(T) | −3.032656 | 1.666 | 4201(−) | 3249(−) | 2433(−) | 2184(−) | 721(−) | 534(−) | 397(−) | 187(−) | 931(−) | 742(−) | 538(−) | 125(−) | 23.22 |
| cc-pVQZ RCCSD(T) | −3.035265 | 1.661 | 4208(−) | 3255(−) | 2451(−) | 2183(−) | 729(−) | 545(−) | 413(−) | 192(−) | 940(−) | 750(−) | 546(−) | 123(−) | 23.35 |
| aug-cc-pVQZ RCCSD(T) | −3.035600 | 1.671 | | | | | | | | | | | | | |
| cc-pVTZ UCCSD(T) | −3.031493 | 1.635 | 4212(74.7) | 3254(781.1) | 2444(3199.7) | 2163(258.3) | 749(285.0) | 545(110.8) | 413(191.9) | 200(25.8) | 953(10.0) | 756(19.9) | 558(369.9) | 123(17.1) | 23.40 |
| aug-cc-pVTZ UCCSD(T) | −3.032657 | 1.666 | 4201(74.9) | 3249(785.7) | 2433(3082.4) | 2184(284.5) | 721(304.1) | 534(100.3) | 397(147.7) | 187(24.1) | 931(9.1) | 742(25.0) | 538(377.0) | 125(15.2) | 23.22 |
| cc-pVQZ UCCSD(T) | −3.035266 | 1.661 | 4208(74.2) | 3255(780.6) | 2451(3152.1) | 2183(263.2) | 729(298.0) | 545(104.3) | 413(153.3) | 192(25.0) | 940(9.0) | 750(22.4) | 546(372.6) | 123(16.1) | 23.35 |
| aug-cc-pVQZ UCCSD(T) | −3.035600 | 1.671 | 4203(74.6) | 3255(783.5) | 2447(3102.4) | 2189(274.2) | 723(304.8) | 543(102.5) | 408(137.9) | 187(24.2) | 935(8.6) | 746(25.0) | 537(376.5) | 124(14.9) | 23.30 |
| cc-pVTZ UCCSDT | −3.031602 | 1.625 | 4210(75.0) | 3251(784.6) | 2440(3206.7) | 2155(263.1) | 752(284.8) | 547(114.2) | 413(193.7) | 201(26.0) | 956(10.1) | 757(19.9) | 559(369.1) | 123(16.8) | 23.39 |

**TABLE 3: Theoretical Predictions of the Total Energy (in Hartree), Harmonic Vibrational Frequencies (in $cm^{-1}$), Infrared Intensities (in parentheses in km $mol^{-1}$), and Zero-Point Vibrational Energy (ZPVE in kcal $mol^{-1}$) for 3, the $\tilde{X}\ ^4A'_1$ Equilibrium Geometry of the $H_6^+$ Molecule in $D_{3h}$ Symmetry (IR intensities for the e′ modes are doubled)**

| theory | energy | $\omega_1(a'_1)$ | $\omega_2(a'_1)$ | $\omega_3(a'_2)$ | $\omega_4(e')$ | $\omega_5(e')$ | $\omega_6(e')$ | $\omega_7(a''_2)$ | $\omega_8(e'')$ | ZPVE |
|---|---|---|---|---|---|---|---|---|---|---|
| cc-pVTZ ROHF | −2.810532 | 3371(0.0) | 393(0.0) | 535(0.0) | 2671(1726.9) | 388(629.2) | 106(13.5) | 154(52.5) | 575(0.0) | 17.06 |
| aug-cc-pVTZ ROHF | −2.811467 | 3378(0.0) | 373(0.0) | 488(0.0) | 2682(1658.4) | 372(565.6) | 104(13.9) | 138(56.1) | 513(0.0) | 16.76 |
| cc-pVQZ ROHF | −2.812150 | 3379(0.0) | 381(0.0) | 509(0.0) | 2681(1696.9) | 379(588.1) | 106(13.3) | 145(53.4) | 542(0.0) | 16.91 |
| aug-cc-pVQZ ROHF | −2.812420 | 3381(0.0) | 374(0.0) | 493(0.0) | 2684(1665.8) | 373(566.7) | 105(13.5) | 139(55.7) | 519(0.0) | 16.80 |
| cc-pVTZ UHF | −2.810605 | 3366(0.0) | 394(0.0) | 538(0.0) | 2667(1741.5) | 380(638.6) | 105(10.9) | 155(52.0) | 578(0.0) | 17.03 |
| aug-cc-pVTZ UHF | −2.811534 | 3373(0.0) | 373(0.0) | 492(0.0) | 2678(1671.9) | 364(573.7) | 104(11.5) | 139(55.7) | 516(0.0) | 16.73 |
| cc-pVQZ UHF | −2.812220 | 3375(0.0) | 381(0.0) | 512(0.0) | 2678(1710.8) | 370(596.5) | 105(10.9) | 146(53.0) | 545(0.0) | 16.88 |
| aug-cc-pVQZ UHF | −2.812488 | 3376(0.0) | 375(0.0) | 496(0.0) | 2680(1679.4) | 365(574.8) | 105(11.1) | 140(55.2) | 523(0.0) | 16.77 |
| cc-pVTZ RCCSD | −2.858426 | 3143(0.0) | 487(0.0) | 660(0.0) | 2442(1999.1) | 439(772.6) | 126(0.2) | 191(31.7) | 687(0.0) | 16.97 |
| aug-cc-pVTZ RCCSD | −2.859725 | 3141(0.0) | 471(0.0) | 608(0.0) | 2445(1930.6) | 427(709.5) | 115(0.0) | 172(35.8) | 629(0.0) | 16.62 |
| cc-pVQZ RCCSD | −2.861304 | 3149(0.0) | 478(0.0) | 629(0.0) | 2454(1976.6) | 434(728.3) | 121(0.1) | 180(32.8) | 656(0.0) | 16.82 |
| aug-cc-pVQZ RCCSD | −2.861692 | 3150(0.0) | 474(0.0) | 615(0.0) | 2456(1941.8) | 433(705.5) | 115(0.0) | 173(35.4) | 634(0.0) | 16.71 |
| cc-pVTZ UCCSD | −2.858428 | 3142(0.0) | 487(0.0) | 660(0.0) | 2442(1999.5) | 438(772.9) | 126(0.2) | 191(31.7) | 687(0.0) | 16.97 |
| aug-cc-pVTZ UCCSD | −2.859727 | 3141(0.0) | 471(0.0) | 608(0.0) | 2445(1930.9) | 426(709.6) | 115(0.0) | 172(35.8) | 629(0.0) | 16.62 |
| cc-pVQZ UCCSD | −2.861304 | 3149(0.0) | 478(0.0) | 629(0.0) | 2454(1976.9) | 434(728.5) | 120(0.1) | 180(32.7) | 656(0.0) | 16.82 |
| aug-cc-pVQZ UCCSD | −2.861715 | 3148(0.0) | 474(0.0) | 613(0.0) | 2454(1942.8) | 431(707.1) | 114(0.0) | 171(35.3) | 635(0.0) | 16.69 |
| cc-pVTZ RCCSD(T) | −2.858778 | 3128(0.0) | 492(0.0) | 666(0.0) | 2431(2019.7) | 441(780.1) | 127(0.5) | 193(30.7) | 693(0.0) | 16.96 |
| aug-cc-pVTZ RCCSD(T) | −2.860099 | 3126(0.0) | 476(0.0) | 615(0.0) | 2433(1951.8) | 429(717.3) | 115(0.1) | 174(34.8) | 636(0.0) | 16.61 |
| cc-pVQZ RCCSD(T) | −2.861688 | 3134(0.0) | 484(0.0) | 635(0.0) | 2442(1998.5) | 437(736.1) | 121(0.2) | 181(31.8) | 662(0.0) | 16.81 |
| aug-cc-pVQZ RCCSD(T) | −2.862106 | 3133(0.0) | 480(0.0) | 620(0.0) | 2442(1964.1) | 434(714.8) | 115(0.1) | 172(34.3) | 641(0.0) | 16.68 |
| cc-pVTZ UCCSD(T) | −2.858779 | 3128(0.0) | 492(0.0) | 666(0.0) | 2431(2019.9) | 441(780.2) | 127(0.5) | 193(30.7) | 693(0.0) | 16.96 |
| aug-cc-pVTZ UCCSD(T) | −2.860100 | 3126(0.0) | 476(0.0) | 615(0.0) | 2433(1951.8) | 429(717.3) | 115(0.2) | 174(34.8) | 636(0.0) | 16.61 |
| cc-pVQZ UCCSD(T) | −2.861689 | 3134(0.0) | 484(0.0) | 635(0.0) | 2442(1930.6) | 437(709.5) | 121(0.0) | 181(35.8) | 662(0.0) | 16.81 |
| aug-cc-pVQZ UCCSD(T) | −2.862107 | 3133(0.0) | 480(0.0) | 620(0.0) | 2442(1964.7) | 434(714.8) | 114(0.2) | 172(34.3) | 642(0.0) | 16.68 |

**TABLE 4: Theoretical Predictions of the Total Energy (in Hartree), Harmonic Vibrational Frequencies (in $cm^{-1}$), and Zero-Point Vibrational Energy (ZPVE in kcal $mol^{-1}$) for 4, the $\tilde{X}\ ^2A_g$ Transition State of the $H_6^+$ Molecule in $D_{2h}$ Symmetry**

| theory | energy | $\omega_1(a_g)$ | $\omega_2(a_g)$ | $\omega_3(a_g)$ | $\omega_4(b_{1g})$ | $\omega_5(b_{1g})$ | $\omega_6(b_{2g})$ | $\omega_7(a_u)$ | $\omega_8(b_{1u})$ | $\omega_9(b_{2u})$ | $\omega_{10}(b_{2u})$ | $\omega_{11}(b_{3u})$ | $\omega_{12}(b_{3u})$ | ZPVE |
|---|---|---|---|---|---|---|---|---|---|---|---|---|---|---|
| cc-pVTZ ROHF | −2.935089 | 4058 | 2024 | 845 | 1321 | 786 | 1072 | 66i | 383 | 1083 | 347 | 3993 | 592 | 23.59 |
| aug-cc-pVTZ ROHF | −2.935377 | 4054 | 2014 | 842 | 1316 | 780 | 1058 | 66i | 376 | 1082 | 343 | 3990 | 585 | 23.50 |
| cc-pVQZ ROHF | −2.936344 | 4053 | 2013 | 840 | 1315 | 781 | 1054 | 66i | 376 | 1079 | 344 | 3988 | 573 | 23.47 |
| aug-cc-pVQZ ROHF | −2.936426 | 4052 | 2012 | 840 | 1309 | 779 | 1051 | 66i | 374 | 1078 | 343 | 3988 | 572 | 23.44 |
| cc-pVTZ UHF | −2.939021 | 4035 | 2089 | 866 | 1275 | 705 | 1074 | 68i | 385 | 958 | 342 | 3945 | 709 | 23.42 |
| aug-cc-pVTZ UHF | −2.939286 | 4031 | 2079 | 863 | 1266 | 699 | 1054 | 68i | 375 | 956 | 338 | 3941 | 703 | 23.31 |
| cc-pVQZ UHF | −2.940276 | 4030 | 2080 | 861 | 1267 | 699 | 1050 | 68i | 376 | 953 | 338 | 3940 | 695 | 23.29 |
| aug-cc-pVQZ UHF | −2.940353 | 4029 | 2078 | 861 | 1259 | 697 | 1045 | 67i | 373 | 952 | 337 | 3939 | 694 | 23.25 |
| cc-pVTZ RCCSD | −3.036526 | 3864 | 2094 | 905 | 1247 | 618 | 1076 | 71i | 393 | 850 | 339 | 3783 | 1008 | 23.13 |
| aug-cc-pVTZ RCCSD | −3.037485 | 3855 | 2085 | 904 | 1231 | 612 | 1048 | 67i | 383 | 850 | 332 | 3775 | 1005 | 22.99 |
| cc-pVQZ RCCSD | −3.040150 | 3861 | 2087 | 903 | 1235 | 613 | 1048 | 69i | 382 | 849 | 334 | 3780 | 1000 | 23.01 |
| aug-cc-pVQZ RCCSD | −3.040129 | 3858 | 2083 | 903 | 1227 | 621 | 1039 | 79i | 379 | 860 | 317 | 3779 | 1004 | 22.97 |
| cc-pVTZ UCCSD | −3.036592 | 3863 | 2095 | 905 | 1246 | 616 | 1076 | 71i | 393 | 848 | 339 | 3782 | 1011 | 23.12 |
| aug-cc-pVTZ UCCSD | −3.037552 | 3854 | 2086 | 904 | 1230 | 610 | 1048 | 67i | 383 | 848 | 332 | 3774 | 1007 | 22.98 |
| cc-pVQZ UCCSD | −3.040217 | 3860 | 2088 | 903 | 1234 | 611 | 1048 | 69i | 382 | 847 | 334 | 3779 | 1003 | 23.00 |
| aug-cc-pVQZ UCCSD | −3.040470 | 3858 | 2084 | 903 | 1220 | 608 | 1038 | 78i | 379 | 845 | 331 | 3777 | 1001 | 22.93 |
| cc-pVTZ RCCSD(T) | −3.037613 | 3856 | 2097 | 906 | 1242 | 605 | 1075 | 71i | 393 | 835 | 337 | 3776 | 1028 | 23.09 |
| aug-cc-pVTZ RCCSD(T) | −3.038614 | 3847 | 2088 | 905 | 1225 | 600 | 1046 | 68i | 382 | 835 | 330 | 3767 | 1024 | 22.94 |
| cc-pVQZ RCCSD(T) | −3.041310 | 3853 | 2090 | 904 | 1229 | 600 | 1046 | 69i | 382 | 834 | 332 | 3773 | 1021 | 22.96 |
| aug-cc-pVQZ RCCSD(T) | −3.041580 | 3851 | 2086 | 904 | 1217 | 598 | 1036 | 78i | 378 | 832 | 330 | 3770 | 1019 | 22.90 |
| cc-pVTZ UCCSD(T) | −3.037615 | 3856 | 2097 | 906 | 1242 | 606 | 1075 | 71i | 393 | 835 | 337 | 3776 | 1028 | 23.09 |
| aug-cc-pVTZ UCCSD(T) | −3.038615 | 3847 | 2088 | 905 | 1226 | 600 | 1046 | 68i | 382 | 835 | 330 | 3767 | 1025 | 22.95 |
| cc-pVQZ UCCSD(T) | −3.041311 | 3853 | 2090 | 904 | 1230 | 601 | 1046 | 69i | 382 | 835 | 332 | 3773 | 1021 | 22.97 |
| aug-cc-pVQZ UCCSD(T) | −3.041576 | 3850 | 2086 | 904 | 1215 | 597 | 1037 | 80i | 378 | 833 | 330 | 3770 | 1019 | 22.91 |
| cc-pVTZ UCCSDT | −3.037835 | 3854 | 2097 | 906 | 1241 | 603 | 1074 | 71i | 392 | 832 | 337 | 3774 | 1030 | 23.07 |

The analogous MRCI wave function is described in terms of NOs by

$$\Psi = 0.971\Phi_1[(1a')^2(2a')^2(3a')] - 0.091\Phi_2[(1a')^2(2a')^{\alpha}(3a')^{\beta}(4a')^{\alpha}] - 0.081\Phi_3[(2a')^2(3a')(1a'')^2] - 0.067\Phi_4[(1a')^2(3a')(4a')^2] + 0.058\Phi_5[(1a')^2(2a')^{\alpha}(3a')^{\alpha}(4a')^{\beta}] - 0.053\Phi_5[(1a')^2(3a')(5a')^2] + \ldots \quad (18)$$

The two dominant excited configurations with CI coefficient greater than 0.08, $\Phi_2$ $[(2a')^2(3a') \rightarrow (2a')(3a')(4a')]$ and $\Phi_3$ $[(1a')^2 \rightarrow (1a'')^2]$, contribute similarly to both the CASSCF and MRCI wave functions.

For transition state **6** the CASSCF wave function is written in terms of NOs as

$$\Psi = 0.986\Phi_1[(1a_1)^2(2a_1)^2(3a_1)] - 0.095\Phi_2[(2a_1)^2(3a_1)(1b_1)^2] - 0.088\Phi_3[(1a_1)^2(3a_1)(1b_2)^2] - 0.082\Phi_4[(1a_1)^2(3a_1)(4a_1)^2] + \ldots \quad (19)$$

The analogous MRCI wave function is described in terms of NOs by

$$\Psi = 0.981\Phi_1[(1a_1)^2(2a_1)^2(3a_1)] - 0.086\Phi_2[(2a_1)^2(3a_1)(1b_1)^2] - 0.082\Phi_3[(1a_1)^2(3a_1)(1b_2)^2] - 0.076\Phi_4[(1a_1)^2(3a_1)(4a_1)^2] + \ldots \quad (20)$$

Transition state **6** has a wave function similar to that for isomer **2**, and the three dominant excited CSFs correspond to the double excitations $\Phi_2$ $[(1a_1)^2 \rightarrow (1b_1)^2]$, $\Phi_3$ $[(2a_1)^2 \rightarrow (1b_2)^2]$, and $\Phi_4$ $[(2a_1)^2 \rightarrow (4a_1)^2]$.

### Geometries

**Isomer 1 ($D_{2d}$ Point Group Symmetry).** The optimized geometry at various levels of theory, for the global minimum **1** is depicted in Figure 1. This structure involves two neutral $H_2$ molecules which symmetrically share one $H_2^+$ cationic molecule, designated as $H_2(H_2^+)H_2$. The $H_a-H_a$ bond distance and $H_2\cdots H_2^+$ intermolecular distance significantly decrease with more advanced treatments of correlation effects, while the $H_b-H_b$ bond distance increases. This feature may be attributed to the doubly excited configurations ($\Phi_2$) in eqs 9 and 10. There the electrons shift from neutral $H_2$ to $H_2^+$ with correlation effects: the occupation numbers of the $1a_1$ and $1b_2$ MOs in eq 1 decrease, whereas the occupation numbers of the $2a_1$ and the next three virtual MOs increase, as shown in Table 7. This effect may be alternatively interpreted as the positive charge in the $H_2^+$ fragment being partially shifted to the two neutral $H_2$ fragments. The $H_a-H_a$ bond distance of **1** is shorter than the H−H bond distance of $H_2^+$, while the $H_b-H_b$ distance of **1** is longer than the H−H bond distance of neutral $H_2$ (see Figure 7). The H−H bond distances are predicted to be the same at the RCCSD and UCCSD and RCCSD(T) and UCCSD(T) levels of theory.

**TABLE 5: Theoretical Predictions of the Total Energy (in Hartree), Dipole Moment (in Debye), Harmonic Vibrational Frequencies (in $cm^{-1}$), and Zero-Point Vibrational Energy (ZPVE in kcal $mol^{-1}$) for 5, the $\tilde{X}\ ^2A'$ Transition State of the $H_6^+$ Molecule in $C_s$ Symmetry**

| theory | energy | $\mu_e$ | $\omega_1(a')$ | $\omega_2(a')$ | $\omega_3(a')$ | $\omega_4(a')$ | $\omega_5(a')$ | $\omega_6(a')$ | $\omega_7(a')$ | $\omega_8(a')$ | $\omega_9(a'')$ | $\omega_{10}(a'')$ | $\omega_{11}(a'')$ | $\omega_{12}(a'')$ | ZPVE |
|---|---|---|---|---|---|---|---|---|---|---|---|---|---|---|---|
| cc-pVTZ ROHF | −2.915977 | 1.080 | 4144 | 2328 | 2069 | 1298 | 816 | 611 | 361 | 2241i | 1166 | 775 | 437 | 116 | 20.19 |
| aug-cc-pVTZ ROHF | −2.916274 | 1.093 | 4141 | 2332 | 2065 | 1296 | 814 | 606 | 361 | 2245i | 1159 | 768 | 423 | 125 | 20.14 |
| cc-pVQZ ROHF | −2.917235 | 1.122 | 4142 | 2347 | 2064 | 1302 | 812 | 606 | 360 | 2242i | 1151 | 766 | 421 | 122 | 20.15 |
| aug-cc-pVQZ ROHF | −2.917320 | 1.121 | 4141 | 2347 | 2064 | 1302 | 812 | 605 | 360 | 2243i | 1149 | 765 | 417 | 122 | 20.14 |
| cc-pVTZ UHF | −2.926486 | 1.189 | 4161 | 2390 | 2038 | 1536 | 771 | 674 | 372 | 1020i | 1118 | 761 | 521 | 112 | 20.66 |
| aug-cc-pVTZ UHF | −2.926780 | 1.205 | 4159 | 2391 | 2036 | 1535 | 767 | 664 | 370 | 1025i | 1110 | 752 | 502 | 120 | 20.60 |
| cc-pVQZ UHF | −2.927770 | 1.223 | 4158 | 2399 | 2034 | 1546 | 767 | 662 | 370 | 1019i | 1105 | 751 | 501 | 117 | 20.60 |
| aug-cc-pVQZ UHF | −2.927856 | 1.222 | 4157 | 2399 | 2034 | 1547 | 766 | 661 | 369 | 1019i | 1103 | 749 | 495 | 117 | 20.58 |
| cc-pVTZ RCCSD | −3.024632 | 1.023 | 4020 | 2373 | 2142 | 1357 | 848 | 823 | 379 | 917i | 1103 | 795 | 653 | 117 | 20.89 |
| aug-cc-pVTZ RCCSD | −3.025599 | 1.016 | 4010 | 2365 | 2134 | 1358 | 842 | 807 | 373 | 918i | 1093 | 780 | 629 | 120 | 20.75 |
| cc-pVQZ RCCSD | −3.028233 | 1.035 | | | | | | | | | | | | | |
| aug-cc-pVQZ RCCSD | −3.028533 | 1.032 | | | | | | | | | | | | | |
| cc-pVTZ UCCSD | −3.024753 | 1.040 | 4023 | 2382 | 2141 | 1356 | 849 | 823 | 378 | 912i | 1100 | 796 | 654 | 117 | 20.90 |
| aug-cc-pVTZ UCCSD | −3.025723 | 1.033 | 4013 | 2374 | 2132 | 1357 | 842 | 808 | 372 | 912i | 1090 | 781 | 631 | 120 | 20.76 |
| cc-pVQZ UCCSD | −3.028360 | 1.052 | 4020 | 2388 | 2135 | 1367 | 845 | 810 | 375 | 905i | 1091 | 783 | 633 | 121 | 20.83 |
| aug-cc-pVQZ UCCSD | −3.028635 | 1.047 | 4017 | 2385 | 2133 | 1367 | 844 | 807 | 373 | 904i | 1088 | 778 | 626 | 122 | 20.79 |
| cc-pVTZ RCCSD(T) | −3.025974 | 1.021 | 4019 | 2383 | 2155 | 1323 | 860 | 830 | 380 | 897i | 1100 | 801 | 663 | 116 | 20.92 |
| aug-cc-pVTZ RCCSD(T) | −3.027010 | 1.013 | 4009 | 2375 | 2145 | 1323 | 852 | 816 | 373 | 898i | 1090 | 785 | 641 | 120 | 20.77 |
| cc-pVQZ RCCSD(T) | −3.029657 | 1.032 | | | | | | | | | | | | | |
| aug-cc-pVQZ RCCSD(T) | −3.029970 | 1.028 | | | | | | | | | | | | | |
| cc-pVTZ UCCSD(T) | −3.025968 | 1.018 | 4019 | 2381 | 2155 | 1324 | 860 | 830 | 380 | 894i | 1101 | 801 | 663 | 116 | 20.92 |
| aug-cc-pVTZ UCCSD(T) | −3.026979 | 1.009 | 4009 | 2371 | 2146 | 1325 | 851 | 817 | 374 | 894i | 1091 | 785 | 641 | 119 | 20.77 |
| cc-pVQZ UCCSD(T) | −3.029650 | 1.029 | 4015 | 2386 | 2150 | 1333 | 854 | 820 | 376 | 887i | 1093 | 787 | 643 | 120 | 20.84 |
| aug-cc-pVQZ UCCSD(T) | −3.029938 | 1.023 | 4012 | 2382 | 2148 | 1333 | 853 | 817 | 375 | 885i | 1089 | 783 | 637 | 121 | 20.80 |

**TABLE 6: Theoretical Predictions of the Total Energy (in Hartree), Dipole Moment (in Debye), Harmonic Vibrational Frequencies (in $cm^{-1}$), and Zero-Point Vibrational Energy (ZPVE in kcal $mol^{-1}$) for 6, the $\tilde{X}\ ^2A_1$ Transition State of the $H_6^+$ Molecule in $C_{2v}$ Symmetry**

| theory | energy | $\mu_e$ | $\omega_1(a_1)$ | $\omega_2(a_1)$ | $\omega_3(a_1)$ | $\omega_4(a_1)$ | $\omega_5(a_1)$ | $\omega_6(a_2)$ | $\omega_7(b_1)$ | $\omega_8(b_1)$ | $\omega_9(b_1)$ | $\omega_{10}(b_2)$ | $\omega_{11}(b_2)$ | $\omega_{12}(b_2)$ | ZPVE |
|---|---|---|---|---|---|---|---|---|---|---|---|---|---|---|---|
| cc-pVTZ ROHF | −2.942826 | 0.383 | 4408 | 3598 | 2564 | 471 | 249 | 161 | 905 | 712 | 92 | 2593 | 521 | 145i | 23.26 |
| aug-cc-pVTZ ROHF | −2.943665 | 0.492 | 4406 | 3584 | 2585 | 457 | 257 | 169 | 875 | 678 | 71 | 2613 | 502 | 120i | 23.15 |
| cc-pVQZ ROHF | −2.944542 | 0.479 | 4404 | 3590 | 2586 | 464 | 266 | 164 | 884 | 690 | 80 | 2610 | 506 | 127i | 23.22 |
| aug-cc-pVQZ ROHF | −2.944783 | 0.493 | 4403 | 3586 | 2589 | 462 | 257 | 167 | 878 | 681 | 68 | 2616 | 505 | 119i | 23.18 |
| cc-pVTZ UHF | −2.942834 | 0.392 | 4408 | 3598 | 2564 | 471 | 249 | 161 | 904 | 712 | 93 | 2592 | 520 | 146i | 23.26 |
| aug-cc-pVTZ UHF | −2.943673 | 0.499 | 4406 | 3584 | 2586 | 457 | 257 | 169 | 875 | 678 | 72 | 2612 | 502 | 121i | 23.15 |
| cc-pVQZ UHF | −2.944550 | 0.486 | 4404 | 3590 | 2587 | 464 | 266 | 164 | 884 | 690 | 81 | 2609 | 506 | 128i | 23.22 |
| aug-cc-pVQZ UHF | −2.944791 | 0.500 | 4403 | 3586 | 2589 | 462 | 257 | 167 | 878 | 681 | 69 | 2615 | 504 | 120i | 23.17 |
| cc-pVTZ RCCSD | −3.028232 | 0.178 | 4179 | 3596 | 2166 | 534 | 281 | 185 | 1052 | 810 | 109 | 2269 | 679 | 176i | 22.67 |
| aug-cc-pVTZ RCCSD | −3.029575 | 0.069 | 4174 | 3571 | 2191 | 522 | 291 | 185 | 1016 | 783 | 87 | 2292 | 655 | 156i | 22.54 |
| cc-pVQZ RCCSD | −3.032069 | 0.049 | 4181 | 3581 | 2210 | 537 | 300 | 185 | 1023 | 791 | 93 | 2304 | 654 | 162i | 22.67 |
| aug-cc-pVQZ RCCSD | −3.032464 | 0.028 | 4179 | 3575 | 2213 | 534 | 294 | 186 | 1015 | 785 | 82 | 2309 | 650 | 157i | 22.62 |
| cc-pVTZ UCCSD | −3.028232 | 0.178 | 4179 | 3596 | 2166 | 534 | 281 | 185 | 1052 | 810 | 109 | 2269 | 679 | 176i | 22.67 |
| aug-cc-pVTZ UCCSD | −3.029578 | 0.069 | 4174 | 3571 | 2191 | 522 | 291 | 185 | 1016 | 785 | 86 | 2292 | 655 | 156i | 22.54 |
| cc-pVQZ UCCSD | −3.032071 | 0.049 | 4181 | 3581 | 2210 | 537 | 299 | 185 | 1023 | 791 | 93 | 2304 | 654 | 162i | 22.67 |
| aug-cc-pVQZ UCCSD | −3.032467 | 0.027 | 4179 | 3575 | 2214 | 534 | 294 | 186 | 1015 | 785 | 83 | 2309 | 649 | 157i | 22.62 |
| cc-pVTZ RCCSD(T) | −3.028745 | 0.290 | 4167 | 3610 | 2104 | 541 | 278 | 187 | 1077 | 823 | 108 | 2230 | 701 | 176i | 22.62 |
| aug-cc-pVTZ RCCSD(T) | −3.030108 | 0.180 | 4161 | 3584 | 2129 | 529 | 289 | 188 | 1042 | 799 | 86 | 2253 | 678 | 157i | 22.50 |
| cc-pVQZ RCCSD(T) | −3.032613 | 0.154 | 4169 | 3593 | 2151 | 544 | 297 | 188 | 1047 | 804 | 93 | 2266 | 676 | 163i | 22.63 |
| aug-cc-pVQZ RCCSD(T) | −3.033016 | 0.132 | 4166 | 3587 | 2154 | 542 | 293 | 189 | 1039 | 798 | 83 | 2271 | 672 | 158i | 22.58 |
| cc-pVTZ UCCSD(T) | −3.028745 | 0.290 | 4167 | 3610 | 2104 | 541 | 278 | 187 | 1077 | 823 | 108 | 2230 | 701 | 176i | 22.62 |
| aug-cc-pVTZ UCCSD(T) | −3.030109 | 0.180 | 4161 | 3584 | 2129 | 529 | 289 | 188 | 1042 | 799 | 86 | 2253 | 678 | 157i | 22.50 |
| cc-pVQZ UCCSD(T) | −3.032613 | 0.154 | 4169 | 3593 | 2151 | 544 | 297 | 187 | 1047 | 804 | 93 | 2266 | 677 | 163i | 22.63 |
| aug-cc-pVQZ UCCSD(T) | −3.033016 | 0.132 | 4166 | 3587 | 2154 | 542 | 293 | 188 | 1039 | 798 | 83 | 2271 | 672 | 158i | 22.58 |

**TABLE 7: Natural Orbital and Sum of Virtual Molecular Orbitals (VMOs) Electron Occupation Numbers for the Valence MOs of CASSCF Wavefunctions at the aug-cc-pVTZ UCCSD(T) Optimized Geometries**

| MO | structure **1** | structure **2** | structure **3** | structure **4** | structure **5** | structure **6** |
|---|---|---|---|---|---|---|
| 1 | 1.985($1a_1$) | 1.977(1a′) | 1.968($1a'_1$) | 1.985($1a_g$) | 1.976(1a′) | 1.977($1a_1$) |
| 2 | 1.969($1b_2$) | 1.967(2a′) | 2.002(1e′) | 1.969($1b_{2u}$) | 1.961(2a′) | 1.967($2a_1$) |
| 3 | 1.002($2a_1$) | 1.000(3a′) | | 1.002($2a_g$) | 0.999(3a′) | 1.000($3a_1$) |
| 4 | 0.020(1e) | 0.023(1a″) | 1.000($2a'_1$) | 0.020($1b_{3u}$) | 0.029(4a′) | 0.023($4a_1$) |
| 5 | 0.018($3a_1$) | 0.016(4a′) | 0.032(2e′) | 0.018($3a_g$) | 0.022(1a″) | 0.017($1b_1$) |
| 6 | 0.007($4a_1$) | 0.016(5a′) | | 0.007($2b_{2u}$) | 0.013(5a′) | 0.016($1b_2$) |
| VMOs | 0.045 | 0.055 | 0.031 | 0.045 | 0.064 | 0.055 |

**Isomer 2 ($C_s$ Point Group Symmetry).** The optimized geometry of structure **2** is presented in Figure 2. This isomer consists of three fragments, H, $H_3^+$, and $H_2$, connected as $H(H_3^+)H_2$. The $H_a-H_c$, $H_a-H_d$, $H_c-H_d$, and $H_b-H_b$ bond distances increase with inclusion of correlation effects, while the $H_d\cdots H_e$ distance and the $H_2\cdots H_3^+$ intermolecular distance drastically decrease. This phenomenon may be attributed to the double excitations in eqs 11 and 12 which move the electrons from neutral $H_2$ to $H_3^+$: the occupation numbers of the 1a′ and 2a′ MOs decrease, while those of the virtual MOs increase, as presented in Table 7.

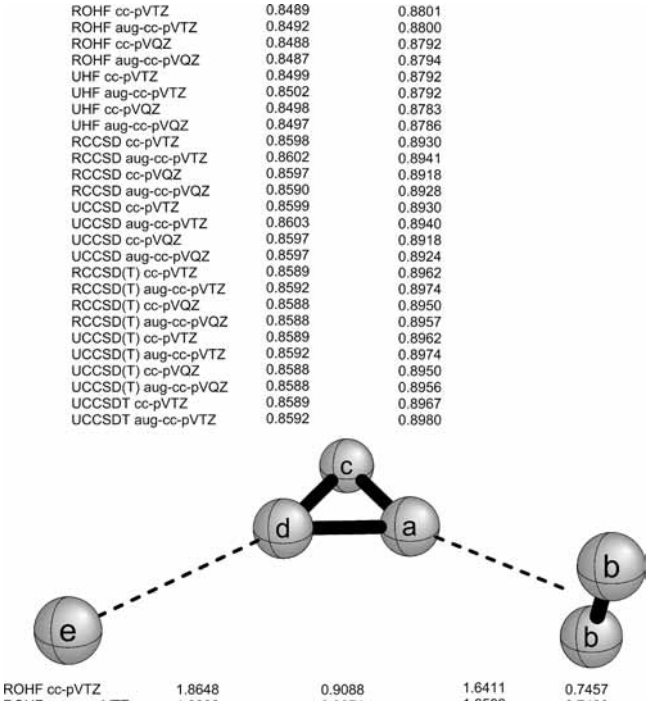


| | | | | |
|---|---|---|---|---|
| ROHF cc-pVTZ | 0.8489 | 0.8801 | | |
| ROHF aug-cc-pVTZ | 0.8492 | 0.8800 | | |
| ROHF cc-pVQZ | 0.8488 | 0.8792 | | |
| ROHF aug-cc-pVQZ | 0.8487 | 0.8794 | | |
| UHF cc-pVTZ | 0.8499 | 0.8792 | | |
| UHF aug-cc-pVTZ | 0.8502 | 0.8792 | | |
| UHF cc-pVQZ | 0.8498 | 0.8783 | | |
| UHF aug-cc-pVQZ | 0.8497 | 0.8786 | | |
| RCCSD cc-pVTZ | 0.8598 | 0.8930 | | |
| RCCSD aug-cc-pVTZ | 0.8602 | 0.8941 | | |
| RCCSD cc-pVQZ | 0.8597 | 0.8918 | | |
| RCCSD aug-cc-pVQZ | 0.8590 | 0.8928 | | |
| UCCSD cc-pVTZ | 0.8599 | 0.8930 | | |
| UCCSD aug-cc-pVTZ | 0.8603 | 0.8940 | | |
| UCCSD cc-pVQZ | 0.8597 | 0.8918 | | |
| UCCSD aug-cc-pVQZ | 0.8597 | 0.8924 | | |
| RCCSD(T) cc-pVTZ | 0.8589 | 0.8962 | | |
| RCCSD(T) aug-cc-pVTZ | 0.8592 | 0.8974 | | |
| RCCSD(T) cc-pVQZ | 0.8588 | 0.8950 | | |
| RCCSD(T) aug-cc-pVQZ | 0.8588 | 0.8957 | | |
| UCCSD(T) cc-pVTZ | 0.8589 | 0.8962 | | |
| UCCSD(T) aug-cc-pVTZ | 0.8592 | 0.8974 | | |
| UCCSD(T) cc-pVQZ | 0.8588 | 0.8950 | | |
| UCCSD(T) aug-cc-pVQZ | 0.8588 | 0.8956 | | |
| UCCSDT cc-pVTZ | 0.8589 | 0.8967 | | |
| UCCSDT aug-cc-pVTZ | 0.8592 | 0.8980 | | |
| ROHF cc-pVTZ | 1.8648 | 0.9088 | 1.6411 | 0.7457 |
| ROHF aug-cc-pVTZ | 1.8866 | 0.9071 | 1.6503 | 0.7460 |
| ROHF cc-pVQZ | 1.8769 | 0.9071 | 1.6487 | 0.7452 |
| ROHF aug-cc-pVQZ | 1.8838 | 0.9068 | 1.6492 | 0.7453 |
| UHF cc-pVTZ | 1.8458 | 0.9094 | 1.6442 | 0.7457 |
| UHF aug-cc-pVTZ | 1.8684 | 0.9077 | 1.6532 | 0.7459 |
| UHF cc-pVQZ | 1.8584 | 0.9077 | 1.6516 | 0.7452 |
| UHF aug-cc-pVQZ | 1.8655 | 0.9074 | 1.6521 | 0.7453 |
| RCCSD cc-pVTZ | 1.6269 | 0.9491 | 1.5063 | 0.7573 |
| RCCSD aug-cc-pVTZ | 1.6409 | 0.9472 | 1.5104 | 0.7579 |
| RCCSD cc-pVQZ | 1.6309 | 0.9465 | 1.5105 | 0.7567 |
| RCCSD aug-cc-pVQZ | 1.6417 | 0.9454 | 1.5096 | 0.7569 |
| UCCSD cc-pVTZ | 1.6264 | 0.9491 | 1.5065 | 0.7573 |
| UCCSD aug-cc-pVTZ | 1.6404 | 0.9473 | 1.5105 | 0.7579 |
| UCCSD cc-pVQZ | 1.6304 | 0.9465 | 1.5106 | 0.7567 |
| UCCSD aug-cc-pVQZ | 1.6351 | 0.9460 | 1.5107 | 0.7569 |
| RCCSD(T) cc-pVTZ | 1.6191 | 0.9540 | 1.4874 | 0.7581 |
| RCCSD(T) aug-cc-pVTZ | 1.6331 | 0.9522 | 1.4903 | 0.7587 |
| RCCSD(T) cc-pVQZ | 1.6221 | 0.9515 | 1.4909 | 0.7575 |
| RCCSD(T) aug-cc-pVQZ | 1.6268 | 0.9510 | 1.4907 | 0.7577 |
| UCCSD(T) cc-pVTZ | 1.6190 | 0.9540 | 1.4874 | 0.7581 |
| UCCSD(T) aug-cc-pVTZ | 1.6330 | 0.9522 | 1.4903 | 0.7587 |
| UCCSD(T) cc-pVQZ | 1.6220 | 0.9515 | 1.4910 | 0.7575 |
| UCCSD(T) aug-cc-pVQZ | 1.6267 | 0.9510 | 1.4908 | 0.7577 |
| UCCSDT cc-pVTZ | 1.6168 | 0.9550 | 1.4846 | 0.7582 |
| UCCSDT aug-cc-pVTZ | 1.6305 | 0.9532 | 1.4873 | 0.7588 |

**Figure 2.** Predicted geometries for **2**, the $\tilde{X}\ ^2A'$ equilibrium geometry of the $H_6^+$ molecule in $C_s$ symmetry (isomer **2**). Bond lengths are in angstroms.

Consider the central triangle in structure **2**. The $H_c-H_d$ bond distance of **2** is shorter than for isolated $H_3^+$ (in Figure 7), while the $H_a-H_c$ and $H_a-H_d$ bond distances are longer. The $H_b-H_b$ bond distance of **2** is longer than that for $H_2$; however, it is shorter than the $H_b-H_b$ bond distance of $H_5^+$ ($C_{2v}$, in Figure 7) and the $H_b-H_b$ bond distance of **1**. The intermolecular distance $H_3^+\cdots H_2$ (1.491 Å at the aug-cc-pVQZ RCCSD(T) level of theory) of **2** is much longer than the intermolecular distance $H_3^+\cdots H_2$ (1.294 Å) of the $H_5^+$ ($C_{2v}$) cluster or the $H_2^+\cdots H_2$ distance (1.159 Å at the same level) of isomer **1**. Consequently, isomer **2** appears to have the weakest intermolecular interaction among the three clusters.

**Isomer 3 ($D_{3h}$ Point Group Symmetry).** The optimized geometry of quartet state **3** is shown in Figure 3. This structure qualitatively incorporates three neutral H atoms and one $H_3^+$ cation. The H−H bond distance of the $H_3^+$ cationic core is slightly longer (0.027 Å) than the H−H bond distance of the $H_3^+$ cationic molecule. This H−H bond distance of the $H_3^+$ cationic core increase, and the $H_a\cdots H_b$ distance of isomer **3** becomes significantly shorter with more complete treatment of correlation. This feature may be due to the fact that some electron density shifts from the $H_3^+$ cationic core to the 2e′ MOs in eqs 13 and 14: the occupation numbers of the $1a'_1$ MO in eq 3 decrease, whereas the 2e′ occupation number increases, as shown in Table 7. In this light, it should be mentioned that the $H_a\cdots H_b$ distance (1.714 Å at the aug-cc-pVQZ RCCSD(T) level) of isomer **3** is longer than the $H_d\cdots H_e$ distance (1.627 Å at the same level) of isomer **2**.

**Transition State 4 ($D_{2h}$ Point Group Symmetry).** The optimized geometry of **4** is shown in Figure 4. Structure **4** represents an isomerization transition state between the two equivalent structures of isomer **1** via an internal rotation about the $H_2\cdots H_2^+\cdots H_2$ axis. The three structural parameters and their variation with basis sets and correlation effects are very similar (to within 0.001 Å) to those of isomer **1**. The total electron occupation number in the virtual orbitals (0.045) for the structure **4** is indeed practically the same as that for isomer **1** (see Table 7).

**Transition State 5 ($C_s$ Point Group Symmetry).** The optimized geometry of structure **5** is illustrated in Figure 5. This structure represents a transition state between the two equilibrium structures, **1** (in $D_{2d}$ symmetry) and **2** (in $C_s$ symmetry). With more complete treatment of correlation, the $H_a-H_c$, $H_c-H_d$, and $H_a\cdots H_d$ bond distances decrease, while the $H_d-H_e$ and $H_b-H_b$ bond distances and $H_4^+\cdots H_2$ intermolecular distance increase. This phenomenon may due to the spin flipped singly excited configuration $\Phi_2$ [(2a′) → (4a′)] and doubly excited configuration $\Phi_3$ [$(1a')^2 \rightarrow (1a'')^2$] in eqs 17 and 18.

The $H_b-H_b$ bond distance (0.773 Å at the aug-cc-pVQZ RCCSD(T) level of theory) is longer than the H−H bond distance (0.742 Å at the aug-cc-pVQZ RCCSD level of theory) for isolated $H_2$. This $H_b-H_b$ bond length for **5** lies between the distances $H_b-H_b$ (0.791 Å) of **1** and $H_b-H_b$ (0.758 Å) of **2**, as

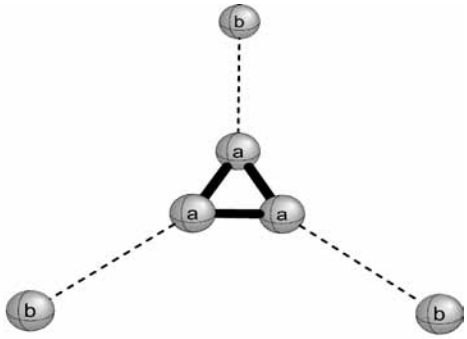


| | | |
|---|---|---|
| ROHF cc-pVTZ | 0.8765 | 1.8811 |
| ROHF aug-cc-pVTZ | 0.8759 | 1.9029 |
| ROHF cc-pVQZ | 0.8756 | 1.8950 |
| ROHF aug-cc-pVQZ | 0.8755 | 1.9007 |
| UHF cc-pVTZ | 0.8768 | 1.8761 |
| UHF aug-cc-pVTZ | 0.8762 | 1.8979 |
| UHF cc-pVQZ | 0.8759 | 1.8900 |
| UHF aug-cc-pVQZ | 0.8758 | 1.8956 |
| RCCSD cc-pVTZ | 0.8948 | 1.7139 |
| RCCSD aug-cc-pVTZ | 0.8949 | 1.7252 |
| RCCSD cc-pVQZ | 0.8937 | 1.7192 |
| RCCSD aug-cc-pVQZ | 0.8937 | 1.7227 |
| UCCSD cc-pVTZ | 0.8948 | 1.7138 |
| UCCSD aug-cc-pVTZ | 0.8950 | 1.7251 |
| UCCSD cc-pVQZ | 0.8937 | 1.7191 |
| UCCSD aug-cc-pVQZ | 0.8938 | 1.7218 |
| RCCSD(T) cc-pVTZ | 0.8958 | 1.7065 |
| RCCSD(T) aug-cc-pVTZ | 0.8960 | 1.7172 |
| RCCSD(T) cc-pVQZ | 0.8948 | 1.7111 |
| RCCSD(T) aug-cc-pVQZ | 0.8949 | 1.7136 |
| UCCSD(T) cc-pVTZ | 0.8958 | 1.7065 |
| UCCSD(T) aug-cc-pVTZ | 0.8960 | 1.7172 |
| UCCSD(T) cc-pVQZ | 0.8948 | 1.7111 |
| UCCSD(T) aug-cc-pVQZ | 0.8949 | 1.7136 |

**Figure 3.** Predicted geometries for **3**, the $\tilde{X}\ ^4A'_1$ equilibrium geometry of the $H_6^+$ molecule in $D_{3h}$ symmetry (isomer **3**). Bond lengths are in angstroms.

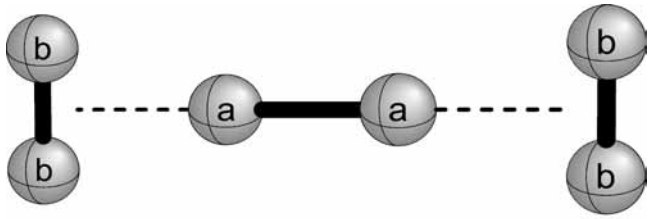


| | | | |
|---|---|---|---|
| ROHF cc-pVTZ | 1.0726 | 1.1813 | 0.7755 |
| ROHF aug-cc-pVTZ | 1.0742 | 1.1814 | 0.7757 |
| ROHF cc-pVQZ | 1.0732 | 1.1821 | 0.7752 |
| ROHF aug-cc-pVQZ | 1.0735 | 1.1820 | 0.7752 |
| UHF cc-pVTZ | 1.0451 | 1.1844 | 0.7779 |
| UHF aug-cc-pVTZ | 1.0463 | 1.1846 | 0.7780 |
| UHF cc-pVQZ | 1.0451 | 1.1853 | 0.7775 |
| UHF aug-cc-pVQZ | 1.0454 | 1.1852 | 0.7776 |
| RCCSD cc-pVTZ | 1.0391 | 1.1599 | 0.7901 |
| RCCSD aug-cc-pVTZ | 1.0408 | 1.1597 | 0.7906 |
| RCCSD cc-pVQZ | 1.0390 | 1.1593 | 0.7897 |
| RCCSD aug-cc-pVQZ | 1.0395 | 1.1586 | 0.7900 |
| UCCSD cc-pVTZ | 1.0387 | 1.1601 | 0.7902 |
| UCCSD aug-cc-pVTZ | 1.0404 | 1.1599 | 0.7907 |
| UCCSD cc-pVQZ | 1.0386 | 1.1594 | 0.7898 |
| UCCSD aug-cc-pVQZ | 1.0391 | 1.1592 | 0.7901 |
| RCCSD(T) cc-pVTZ | 1.0383 | 1.1596 | 0.7907 |
| RCCSD(T) aug-cc-pVTZ | 1.0401 | 1.1593 | 0.7913 |
| RCCSD(T) cc-pVQZ | 1.0383 | 1.1589 | 0.7904 |
| RCCSD(T) aug-cc-pVQZ | 1.0388 | 1.1586 | 0.7906 |
| UCCSD(T) cc-pVTZ | 1.0384 | 1.1596 | 0.7907 |
| UCCSD(T) aug-cc-pVTZ | 1.0402 | 1.1593 | 0.7913 |
| UCCSD(T) cc-pVQZ | 1.0383 | 1.1589 | 0.7904 |
| UCCSD(T) aug-cc-pVQZ | 1.0390 | 1.1589 | 0.7905 |
| UCCSDT cc-pVTZ | 1.0383 | 1.1597 | 0.7909 |
| UCCSDT aug-cc-pVTZ | 1.0401 | 1.1594 | 0.7914 |

**Figure 4.** Predicted geometries for **4**, the $\tilde{X}\ ^2A_g$ transition state of the $H_6^+$ molecule in $D_{2h}$ symmetry (transition state **4**). Bond lengths are in angstroms.

expected. Similarly, the $H_2\cdots H_a$ separation (1.262 Å) falls between $H_2\cdots H_a$ (1.159 Å) for **1** and $H_2\cdots H_a$ (1.491 Å) for **2**.

| | | |
|---|---|---|
| ROHF cc-pVTZ | 0.9795 | 0.9455 |
| ROHF aug-cc-pVTZ | 0.9802 | 0.9452 |
| ROHF cc-pVQZ | 0.9809 | 0.9435 |
| ROHF aug-cc-pVQZ | 0.9808 | 0.9436 |
| UHF cc-pVTZ | 0.9658 | 0.9329 |
| UHF aug-cc-pVTZ | 0.9666 | 0.9327 |
| UHF cc-pVQZ | 0.9671 | 0.9317 |
| UHF aug-cc-pVQZ | 0.9671 | 0.9318 |
| RCCSD cc-pVTZ | 0.9484 | 0.9260 |
| RCCSD aug-cc-pVTZ | 0.9497 | 0.9271 |
| RCCSD cc-pVQZ | 0.9492 | 0.9252 |
| RCCSD aug-cc-pVQZ | 0.9495 | 0.9255 |
| UCCSD cc-pVTZ | 0.9485 | 0.9250 |
| UCCSD aug-cc-pVTZ | 0.9499 | 0.9261 |
| UCCSD cc-pVQZ | 0.9494 | 0.9242 |
| UCCSD aug-cc-pVQZ | 0.9496 | 0.9247 |
| RCCSD(T) cc-pVTZ | 0.9460 | 0.9250 |
| RCCSD(T) aug-cc-pVTZ | 0.9474 | 0.9262 |
| RCCSD(T) cc-pVQZ | 0.9468 | 0.9243 |
| RCCSD(T) aug-cc-pVQZ | 0.9472 | 0.9246 |
| UCCSD(T) cc-pVTZ | 0.9459 | 0.9253 |
| UCCSD(T) aug-cc-pVTZ | 0.9473 | 0.9266 |
| UCCSD(T) cc-pVQZ | 0.9468 | 0.9245 |
| UCCSD(T) aug-cc-pVQZ | 0.9471 | 0.9251 |
| UCCSDT cc-pVTZ | 0.9456 | 0.9250 |
| UCCSDT aug-cc-pVTZ | 0.9470 | 0.9264 |

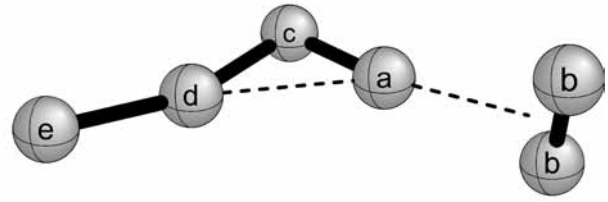


| | | | | |
|---|---|---|---|---|
| ROHF cc-pVTZ | 0.8904 | 1.5238 | 1.2528 | 0.7664 |
| ROHF aug-cc-pVTZ | 0.8909 | 1.5235 | 1.2562 | 0.7664 |
| ROHF cc-pVQZ | 0.8898 | 1.5218 | 1.2608 | 0.7656 |
| ROHF aug-cc-pVQZ | 0.8898 | 1.5218 | 1.2609 | 0.7658 |
| UHF cc-pVTZ | 0.9245 | 1.5103 | 1.2738 | 0.7645 |
| UHF aug-cc-pVTZ | 0.9247 | 1.5102 | 1.2775 | 0.7646 |
| UHF cc-pVQZ | 0.9227 | 1.5108 | 1.2803 | 0.7640 |
| UHF aug-cc-pVQZ | 0.9227 | 1.5110 | 1.2804 | 0.7640 |
| RCCSD cc-pVTZ | 0.9766 | 1.3714 | 1.2580 | 0.7732 |
| RCCSD aug-cc-pVTZ | 0.9764 | 1.3719 | 1.2586 | 0.7738 |
| RCCSD cc-pVQZ | 0.9743 | 1.3704 | 1.2605 | 0.7727 |
| RCCSD aug-cc-pVQZ | 0.9745 | 1.3705 | 1.2605 | 0.7728 |
| UCCSD cc-pVTZ | 0.9784 | 1.3673 | 1.2610 | 0.7729 |
| UCCSD aug-cc-pVTZ | 0.9782 | 1.3679 | 1.2616 | 0.7734 |
| UCCSD cc-pVQZ | 0.9762 | 1.3663 | 1.2636 | 0.7724 |
| UCCSD aug-cc-pVQZ | 0.9761 | 1.3668 | 1.2633 | 0.7726 |
| RCCSD(T) cc-pVTZ | 0.9872 | 1.3554 | 1.2600 | 0.7732 |
| RCCSD(T) aug-cc-pVTZ | 0.9872 | 1.3553 | 1.2605 | 0.7738 |
| RCCSD(T) cc-pVQZ | 0.9852 | 1.3538 | 1.2623 | 0.7727 |
| RCCSD(T) aug-cc-pVQZ | 0.9854 | 1.3537 | 1.2624 | 0.7729 |
| UCCSD(T) cc-pVTZ | 0.9869 | 1.3562 | 1.2594 | 0.7733 |
| UCCSD(T) aug-cc-pVTZ | 0.9866 | 1.3569 | 1.2595 | 0.7738 |
| UCCSD(T) cc-pVQZ | 0.9849 | 1.3548 | 1.2616 | 0.7728 |
| UCCSD(T) aug-cc-pVQZ | 0.9848 | 1.3553 | 1.2612 | 0.7730 |
| UCCSDT cc-pVTZ | 0.9890 | 1.3531 | 1.2604 | 0.7733 |
| UCCSDT aug-cc-pVTZ | 0.9887 | 1.3539 | 1.2604 | 0.7736 |

**Figure 5.** Predicted geometries for **5**, the $\tilde{X}\ ^2A'$ transition state of the $H_6^+$ molecule in $C_s$ symmetry (transition state **5**). Bond lengths are in angstroms.

**Transition State 6 ($C_{2v}$ Point Group Symmetry).** The optimized geometry for **6** is depicted in Figure 6. Structure **6** represents an isomerization transition state between the two equivalent forms of isomer **2** in terms of an inversion motion of the $H_d$ atom in the $H_3^+$ plane. The $H_d\cdots H_3^+$ distance for the transition state **6** is significantly longer compared to the corresponding distance of **2**, while the $H_2\cdots H_3^+$ intermolecular distance is shorter. The $H_c-H_c$ distance of the $H_3^+$ fragment is shorter than that for isolated $H_3^+$ (in Figure 7), whereas the $H_a-H_c$ distance is considerably longer. However, the total electron occupation number in the virtual space (0.055) for the transition state **6** is essentially the same as that for isomer **2** (see Table 7).

## Dipole Moments

For charged molecules, we define the dipole moment with respect to the center of mass. Structures **1**, **3**, and **4** have vanishing dipole moments due to their molecular symmetries. The dipole moment of **2** presented in Table 2 markedly decreases with advanced treatments of correlation effects. The 1a′ MO describes the $\sigma$ bonding of the $H_3^+$ fragment, while the 1a″ MO is an out-of-plane orbital. The double excitation $(1a')^2 \rightarrow (1a'')^2$ in eqs 11 and 12, therefore, diminishes the polarization of the molecule, since the direction of dipole moment is almost

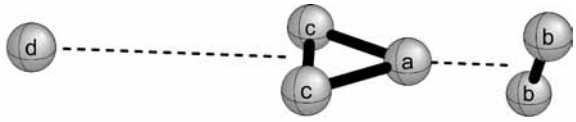


| | | | | | |
|---|---|---|---|---|---|
| ROHF cc-pVTZ | 2.4791 | 0.8317 | 0.9024 | 1.6279 | 0.7473 |
| ROHF aug-cc-pVTZ | 2.4950 | 0.8338 | 0.9001 | 1.6460 | 0.7473 |
| ROHF cc-pVQZ | 2.4770 | 0.8328 | 0.9000 | 1.6426 | 0.7466 |
| ROHF aug-cc-pVQZ | 2.4947 | 0.8333 | 0.8996 | 1.6455 | 0.7466 |
| UHF cc-pVTZ | 2.4734 | 0.8317 | 0.9024 | 1.6283 | 0.7473 |
| UHF aug-cc-pVTZ | 2.4899 | 0.8338 | 0.9001 | 1.6463 | 0.7472 |
| UHF cc-pVQZ | 2.4718 | 0.8328 | 0.8999 | 1.6430 | 0.7466 |
| UHF aug-cc-pVQZ | 2.4896 | 0.8333 | 0.8995 | 1.6458 | 0.7466 |
| RCCSD cc-pVTZ | 2.3468 | 0.8235 | 0.9422 | 1.4515 | 0.7612 |
| RCCSD aug-cc-pVTZ | 2.3571 | 0.8260 | 0.9393 | 1.4654 | 0.7613 |
| RCCSD cc-pVQZ | 2.3386 | 0.8252 | 0.9368 | 1.4681 | 0.7601 |
| RCCSD aug-cc-pVQZ | 2.3487 | 0.8259 | 0.9363 | 1.4708 | 0.7602 |
| UCCSD cc-pVTZ | 2.3467 | 0.8235 | 0.9422 | 1.4516 | 0.7612 |
| UCCSD aug-cc-pVTZ | 2.3570 | 0.8260 | 0.9393 | 1.4654 | 0.7613 |
| UCCSD cc-pVQZ | 2.3385 | 0.8252 | 0.9368 | 1.4681 | 0.7601 |
| UCCSD aug-cc-pVQZ | 2.3479 | 0.8259 | 0.9363 | 1.4708 | 0.7602 |
| RCCSD(T) cc-pVTZ | 2.3476 | 0.8214 | 0.9488 | 1.4295 | 0.7624 |
| RCCSD(T) aug-cc-pVTZ | 2.3567 | 0.8239 | 0.9459 | 1.4427 | 0.7624 |
| RCCSD(T) cc-pVQZ | 2.3375 | 0.8232 | 0.9431 | 1.4462 | 0.7612 |
| RCCSD(T) aug-cc-pVQZ | 2.3463 | 0.8239 | 0.9425 | 1.4488 | 0.7613 |
| UCCSD(T) cc-pVTZ | 2.3476 | 0.8214 | 0.9488 | 1.4295 | 0.7624 |
| UCCSD(T) aug-cc-pVTZ | 2.3567 | 0.8239 | 0.9459 | 1.4427 | 0.7624 |
| UCCSD(T) cc-pVQZ | 2.3374 | 0.8232 | 0.9431 | 1.4462 | 0.7612 |
| UCCSD(T) aug-cc-pVQZ | 2.3463 | 0.8239 | 0.9425 | 1.4488 | 0.7613 |
| UCCSDT cc-pVTZ | 2.3469 | 0.8211 | 0.9500 | 1.4262 | 0.7625 |
| UCCSDT aug-cc-pVTZ | 2.3558 | 0.8236 | 0.9470 | 1.4392 | 0.7626 |

**Figure 6.** Predicted geometries for **6**, the $\tilde{X}\ ^2A_1$ transition state of the $H_6^+$ molecule in $C_{2v}$ symmetry (transition state **6**). Bond lengths are in angstroms.

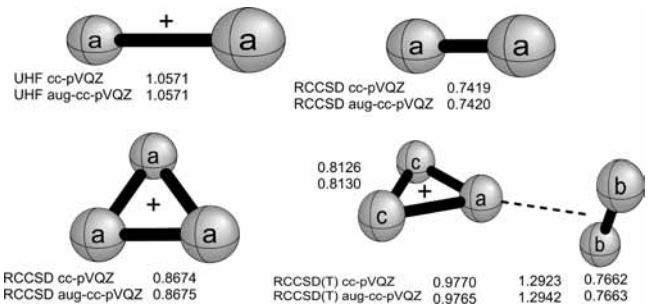


**Figure 7.** Predicted geometries for the ground states of the isolated $H_2^+$, $H_2$, $H_3^+$, and $H_5^+$ molecules. Bond lengths are in angstroms.

parallel to the $H_a-H_c$ axis in the molecular plane. With our most reliable method, aug-cc-pVQZ RCCSD(T), the dipole moment of isomer **2** is predicted to be 1.671 D.

The dipole moment of structure **5**, which is an isomerization transition state between **1** and **2**, is predicted to be 1.028 D at the aug-cc-pVQZ RCCSD(T) level of theory. The magnitude of this dipole moment is about 0.64 D smaller than that for **2**.

Structure **6** in $C_{2v}$ symmetry is an inversion transition state for the two equivalent equilibrium structures **2**. The dipole moment of **6** is quite sensitive to the basis set and treatment of correlation effects. Since the direction of the dipole moment for **6** is along the $C_2$ axis as $^+H\cdot H_3\cdot H_2^-$, its magnitude is determined by the relative charge separation between the $H_a$ and $H_d$ atoms. Consequently, the $\Phi_4$ $[(2a_1)^2 \rightarrow (4a_1)^2]$ double excitation in eqs 19 and 20 is mainly responsible for the decrease in the magnitude with increasing treatment of correlation effects.

## Harmonic Vibrational Frequencies and Infrared (IR) Intensities

**Isomer 1 (see Table 1).** The two vibrational frequencies $\omega_1(a_1)$ (3849 $cm^{-1}$ at the aug-cc-pVQZ CCSD(T) level of theory) and $\omega_5(b_2)$ (3769 $cm^{-1}$) modes are assigned to the H−H stretching frequencies of the $H_2$ fragments, while the $\omega_2(a_1)$ (2087 $cm^{-1}$) mode is associated with the H−H stretching frequency of the central $H_2^+$ moiety. These frequencies are significantly lower than the corresponding frequencies at 4400 $cm^{-1}$ (with the aug-cc-pVQZ CCSD method) for isolated $H_2$ and 2323 $cm^{-1}$ (with the aug-cc-pVQZ UHF method) for $H_2^+$, respectively. The remaining nine low-frequency vibrations arise from the complexation. Among those nine vibrations the $\omega_3(a_1)$ and $\omega_6(b_2)$ frequencies are of special importance, since they closely reflect the strength of association. The vibrational frequencies of the $\omega_3(a_1)$ and $\omega_6(b_2)$ modes become significantly higher with inclusion of correlation effects, due to the shortening of the $H_2\cdots H_2^+$ separation. With the aug-cc-pVQZ basis set the $\omega_3(a_1)$ and $\omega_6(b_2)$ frequencies are 840 and 574 $cm^{-1}$ at the ROHF level of theory, while they are 904 and 1020 $cm^{-1}$ with RCCSD(T). On the other hand, the degenerate rocking motion $[\omega_7(e)]$ of the $H_2^+$ fragment gives rise to the highest vibrational frequency among the remaining six modes. The intensities of the IR active modes ($b_2$ and e symmetry) are considerable.

**Isomer 2 (see Table 2).** The $H_b-H_b$ stretching frequency ($\omega_1(a') = 4203$ $cm^{-1}$ with the aug-cc-pVQZ CCSD(T) method) for **2** is lower than the corresponding frequency (4400 $cm^{-1}$) of the isolated $H_2$ molecule, but it is higher than the $H_b-H_b$ stretching frequency (3849 $cm^{-1}$ with the same method) for **1**. The next three high energy frequencies ($\omega_2$, $\omega_3$, and $\omega_4$) are associated with the H−H stretching modes of the $H_3^+$ fragment. The remaining eight frequencies may be attributed to the vibrational modes due to the complexation. The two stretching vibrational frequencies for the intermolecular interactions in **2**, $H_2\cdots H_3^+$ [$\omega_6(a') = 543$ $cm^{-1}$] and the $H_e\cdots H_3^+$ [$\omega_7(a') = 408$ $cm^{-1}$], are significantly lower than the corresponding frequencies for the two intermolecular interactions in structure **1**, $H_2\cdots H_3^+$ [$\omega_3(a_1) = 904$, $\omega_6(b_2) = 1020$ $cm^{-1}$]. All 12 vibrational modes are IR active for isomer **2** because of the low symmetry. The three H−H stretching modes ($\omega_2-\omega_4$) of the $H_3^+$ fragment show the strongest IR intensities.

**Isomer 3 (see Table 3).** The $\omega_1(a')$ and $\omega_4(e')$ frequencies are assigned to the H−H stretching modes of the $H_3^+$ fragment. Since the central H−H distances are elongated by the complexation, these two frequencies are lower than the corresponding frequencies for the isolated $H_3^+$ molecule. The two outer modes $\omega_2(a'_1)$ and $\omega_5(e')$ are associated with the $H\cdots H_3^+$ interactions. These frequencies increase in magnitude with inclusion of correlation effects due to the noticeable decrease of the $H\cdots H_3^+$ distance. For isomer **3** only e′-symmetry ($\omega_4-\omega_6$) and a″$_2$-symmetry ($\omega_7$) modes are IR active. Among the four IR active vibrations the $\omega_4$ mode has the strongest intensity.

**Transition State 4 (see Table 4).** The $\omega_7(a_u)$ mode for an internal rotation along the $H_2\cdots H_2^+\cdots H_2$ axis possesses an imaginary vibrational frequency, confirming that this structure is a transition state for internal rotation. The magnitude of the $\omega_7$ frequency is relatively small and slightly increases with inclusion of correlation effects, reflecting a shortened $H_2^+\cdots H_2$ distance. The other real vibrational frequencies are very close to those for the global minimum **1**.

**Transition State 5 (see Table 5).** The $\omega_8(a')$ mode of **5** (admixture of $H_e-H_d$ stretching, $H_aH_cH_d$ bending, and $H_a-H_b$ stretching motion) possesses an imaginary vibrational frequency, characterizing it as a transition state between the two equilibrium structures **1** and **2**. The magnitude of $\omega_8$ drastically decreases with inclusion of correlation effects. The $H_b-H_b$ stretching frequency of **5** (4012 $cm^{-1}$) lies between the corresponding

**TABLE 8: Focal Point Analysis of the Relative Energy (in kcal mol$^{-1}$) between Isomers 1 and 2[a]**

| basis set | $\Delta E$[HF] | $+\delta$ [CCSD] | $+\delta$ [CCSD(T)] | $+\delta$ [CCSDT] | $+\delta$ [CCSDTQ] | $+\delta$ [FCI] | $= \Delta E$ |
|---|---|---|---|---|---|---|---|
| cc-pVDZ | −3.69 | +8.83 | +0.29 | +0.08 | +0.00 | +0.00 | [+5.50] |
| cc-pVTZ | −5.35 | +8.89 | +0.34 | +0.07 | +0.00 | +0.00 | [+3.95] |
| cc-pVQZ | −5.52 | +8.99 | +0.36 | +0.07 | [+0.00] | [+0.00] | [+3.90] |
| cc-pV5Z | −5.56 | +9.00 | +0.36 | [+0.07] | [+0.00] | [+0.00] | [+3.87] |
| cc-pV6Z | −5.56 | +9.01 | +0.36 | [+0.07] | [+0.00] | [+0.00] | [+3.88] |
| CBS LIMIT | [−5.57] | [+9.02] | [+0.36] | [+0.07] | [+0.00] | [+0.00] | **[+3.89]** |

[a] The symbol $\delta$ denotes the increment in the relative energy ($\Delta E$) with respect to the preceding level of theory in the hierarchy ROHF → CCSD → CCSD(T) → CCSDT → CCSDTQ → FCI. Square brackets signify results obtained from basis set extrapolations or additivity assumptions. Final prediction is boldfaced.

**TABLE 9: Focal Point Analysis of the Energy Difference (in kcal mol$^{-1}$) between Isomers 1 and 3**

| basis set | $\Delta E$[HF] | $+\delta$ [CCSD] | $+\delta$ [CCSD(T)] | $+\delta$ [CCSDT] | $+\delta$ [CCSDTQ] | $+\delta$ [FCI] | $= \Delta E$ |
|---|---|---|---|---|---|---|---|
| cc-pVDZ | +80.17 | +30.79 | +0.39 | +0.09 | +0.01 | +0.00 | [+111.45] |
| cc-pVTZ | +78.57 | +33.22 | +0.46 | +0.09 | +0.01 | +0.00 | [+112.35] |
| cc-pVQZ | +78.42 | +33.84 | +0.49 | +0.08 | [+0.01] | [+0.00] | [+112.84] |
| cc-pV5Z | +78.38 | +33.99 | +0.49 | [+0.08] | [+0.01] | [+0.00] | [+112.95] |
| cc-pV6Z | +78.37 | +34.05 | +0.49 | [+0.08] | [+0.01] | [+0.00] | [+113.00] |
| CBS LIMIT | [+78.36] | [+34.13] | [+0.50] | [+0.08] | [+0.01] | [+0.00] | **[+113.08]** |

**TABLE 10: Focal Point Analysis of the $H_6^+$ Isomerization Reaction Barrier (in kcal mol$^{-1}$) between Isomers 1 and 2**

| basis set | $\Delta E$[HF] | $+\delta$ [CCSD] | $+\delta$ [CCSD(T)] | $+\delta$ [CCSDT] | $+\delta$ [CCSDTQ] | $+\delta$ [FCI] | $= \Delta E$ |
|---|---|---|---|---|---|---|---|
| cc-pVDZ | +8.97 | −1.71 | −0.12 | −0.02 | −0.01 | +0.00 | [+7.10] |
| cc-pVTZ | +9.05 | −1.56 | −0.16 | −0.02 | −0.01 | +0.00 | [+7.30] |
| cc-pVQZ | +9.02 | −1.52 | −0.16 | −0.02 | [−0.01] | [+0.00] | [+7.31] |
| cc-pV5Z | +9.02 | −1.50 | −0.17 | [−0.02] | [−0.01] | [+0.00] | [+7.32] |
| cc-pV6Z | +9.01 | −1.50 | −0.17 | [−0.02] | [−0.01] | [+0.00] | [+7.32] |
| CBS LIMIT | [+9.01] | [−1.49] | [−0.17] | [−0.02] | [−0.01] | [+0.00] | **[+7.33]** |

**TABLE 11: Focal Point Analysis (kcal mol$^{-1}$) of the $H_6^+$ (in $D_{2d}$ Symmetry, Isomer 1) Dissociation Reaction [$H_6^+$ ($D_{2d}$) → $2H_2 + H_2^+$]**

| basis set | $\Delta E$[HF] | $+\delta$ $E$[CCSD] | $+\delta$ [CCSD(T)] | $+\delta$ [CCSDT] | $+\delta$ [CCSDTQ] | $+\delta$ [FCI] | $= \Delta E$ |
|---|---|---|---|---|---|---|---|
| cc-pVDZ | +43.22 | +14.23 | +0.52 | +0.13 | +0.01 | +0.00 | [+58.11] |
| cc-pVTZ | +41.67 | +14.60 | +0.68 | +0.14 | +0.01 | +0.00 | [+57.09] |
| cc-pVQZ | +41.64 | +14.89 | +0.73 | +0.14 | [+0.01] | [+0.00] | [+57.40] |
| cc-pV5Z | +41.64 | +14.80 | +0.74 | [+0.14] | [+0.01] | [+0.00] | [+57.32] |
| cc-pV6Z | +41.66 | +14.95 | +0.74 | [+0.14] | [+0.01] | [+0.00] | [+57.50] |
| CBS LIMIT | [+41.66] | [+15.16] | [+0.75] | [+0.14] | [+0.01] | [+0.00] | **[+57.72]** |

**TABLE 12: Focal Point Analysis (kcal mol$^{-1}$) of the $H_6^+$ (in $C_s$ Symmetry, Isomer 2) Dissociation Reaction [$H_6^+$ ($C_s$) → $H_3^+ + H_2 + H$]**

| basis set | $\Delta E$[HF] | $+\delta$ [CCSD] | $+\delta$ [CCSD(T)] | $+\delta$ [CCSDT] | $+\delta$ [CCSDTQ] | $+\delta$ [FCI] | $= \Delta E$ |
|---|---|---|---|---|---|---|---|
| cc-pVDZ | +6.64 | +3.61 | +0.24 | +0.06 | +0.01 | +0.00 | [+10.54] |
| cc-pVTZ | +6.71 | +4.57 | +0.35 | +0.07 | +0.01 | +0.00 | [+11.71] |
| cc-pVQZ | +6.93 | +4.72 | +0.37 | +0.07 | [+0.01] | [+0.00] | [+12.10] |
| cc-pV5Z | +6.97 | +4.70 | +0.38 | [+0.07] | [+0.01] | [+0.00] | [+12.12] |
| cc-pV6Z | +6.99 | +4.78 | +0.38 | [+0.07] | [+0.01] | [+0.00] | [+12.23] |
| CBS LIMIT | [+6.99] | [+4.90] | [+0.39] | [+0.07] | [+0.01] | [+0.00] | **[+12.35]** |

frequencies of the global minimum **1** (3849 cm$^{-1}$) and structure **2** (4203 cm$^{-1}$), reflecting the respective $H_b-H_b$ bond distances.

**Transition State 6 (see Table 6).** The $\omega_{12}(b_2)$ mode for a $H_d\cdots H_3^+\cdots H_2$ bending motion displays an imaginary vibrational frequency, indicating a transition state between the two equivalent equilibrium $C_s$ structures **2**. The $H_b-H_b$ stretching frequency ($\omega_1(a_1) = 4166$ cm$^{-1}$) of the transition state **6** is lower than the corresponding frequency [$\omega_1(a') = 4203$ cm$^{-1}$] of **2** due to the longer $H_b-H_b$ bond distance. On the other hand, the $H_c-H_c$ stretching frequency [$\omega_2(a_1) = 3587$ cm$^{-1}$] of **6** is higher than the corresponding frequency [$\omega_2(a') = 3255$ cm$^{-1}$] of **2**, reflecting the shorter $H_c-H_c$ bond length. The $\omega_5$ frequency (293 cm$^{-1}$) for the $H_d\cdots H_3^+$ stretching mode is significantly lower than the corresponding $\omega_7$ frequency (408 cm$^{-1}$) of isomer **2**.

## Energetics

The total energies for the six $H_6^+$ structures are presented in Tables 1−6. Focal point analyses for various relative energies between the six structures are provided in Tables 8−12. The DBOC contribution to the energy differences is relatively small (no more than 0.12 kcal mol$^{-1}$, as shown in Table 13), with estimated uncertainty of ±0.01 kcal mol$^{-1}$.[48,66,67] Thus, employing the DBOC to treat non-adiabatic effects should be sufficient to obtain the precision reported herein.

**Energy Difference between Isomers 1 and 2.** The focal point analysis for the energy separation between **1** and **2** is shown in Table 8. At the ROHF level of theory, **2** is falsely predicted to be the lowest-lying isomer, the energy difference being 5.6 kcal mol$^{-1}$ at the CBS limit. Inclusion of correlation effects, however, reverses

**TABLE 13: Relative Energies of the Six $H_6^+$ Structures According to the Focal Point Analyses, Energies in kcal mol$^{-1}$**

| | 1 | 2 | 3 | 4 | 5 | 6 |
|---|---|---|---|---|---|---|
| $\Delta E$ | 0.00 | 3.89 | 113.08 | 0.03 | 7.33 | 5.52 |
| $\Delta E_Z$[a] | 0.00 | 4.18 | 106.88 | −0.07 | 5.12 | 5.09 |
| $\Delta E_{ZD}$[b] | 0.00 | 4.16 | 106.92 | −0.07 | 5.24 | 5.07 |

[a] Relative energies with the zero-point vibrational energy corrections. [b] Relative energies with the zero-point vibrational energy and diagonal Born−Oppenheimer corrections.

the energy ordering and predicts structure **1** to be the global minimum. This feature may be mainly attributed to the electron density shift from the two $H_2$ fragments ($1b_2$ MO) to the $H_2^+$ ($2a_1$ MO) fragment, as shown in Table 7.

The increments of energy difference beyond the ROHF approximation are +9.02[CCSD], +0.36[CCSD(T)], +0.07[CCSDT], +0.00[CCSDTQ], and +0.00 kcal mol$^{-1}$ (FCI). The marked increment at the CCSD level of theory is in agreement with the pronounced predicted blue shifts of the two $H_2\cdots H_2^+\cdots H_2$ stretching frequencies [$\omega_3(a_1)$ and $\omega_6(b_2)$]. Since the $H_6^+$ cluster has only five electrons, the correlation effects beyond triple excitations appear to be small. Although the cc-pVDZ basis set alone is inadequate for a precise description of relative energy, very little basis set sensitivity is observed with larger bases; the cc-pVDZ, however, is able to describe the higher-order excitations effectually as demonstrated by the CCSDT−CCSD(T) increments computed with the cc-pVDZ and cc-pVTZ basis sets. At the FCI-CBS limit isomer **2** is predicted to lie 3.9 ± 0.1 kcal mol$^{-1}$ above isomer **1**.

**Energy Separation between Isomers 1 and 3.** Our focal point analysis for the energy difference between **1** and **3** is presented in Table 9. At all levels of theory structure **3** is determined to be higher lying than **1**. The CCSD-HF energy increment (+34.1 kcal mol$^{-1}$ at the CBS limit) is much larger than the corresponding value for the **1** − **2** energy separation value (+9.0 kcal mol$^{-1}$ at the CBS limit) in Table 8, due to the difference in spin multiplicity; the in balance in the number of paired electrons results in different correlation energies for the two species, since correlation is primarily an opposite spin phenomenon. As before, very little basis set sensitivity is observed for the reaction energy. At the FCI-CBS limit the quartet isomer **3** is predicted to lie 113.1 ± 0.1 kcal mol$^{-1}$ above isomer **1**.

**Energy Barrier for the Isomerization Reaction between 1 and 2.** The energy barrier for the forward isomerization reaction

$$\mathbf{1}(\text{equil}) \rightarrow \mathbf{5}(\text{TS}) \rightarrow \mathbf{2}(\text{equil}) \quad (21)$$

based on the FPA is provided in Table 10. At the ROHF level of theory, the barrier height is predicted to be 9.0 kcal mol$^{-1}$. With inclusion of correlation effects the transition state (structure **5**) is preferentially stabilized relative to **1**. This finding is supported by the fact that the total electron occupation number in the virtual MOs (0.064) for the transition states (structure **5**) is noticeably larger than the corresponding value (0.045) for the global minimum **1**. The final barrier height for the isomerization reaction is predicted to be 7.3 ± 0.1 kcal mol$^{-1}$ at the FCI-CBS limit. Using the results in Tables 8 and 10, the energy barrier for the reverse isomerization reaction (isomer **2** → isomer **1**) is predicted to be 3.4 ± 0.1 kcal mol$^{-1}$.

**Dissociation Energy for the Global Minimum 1.** The energy for the fragmentation of **1**

$$H_6^+(D_{2d}) \rightarrow 2H_2 + H_2^+ \quad (22)$$

based on the FPA is displayed in Table 11. With the HF method the equilibrium dissociation energy ($D_e$) is computed to be 41.7 kcal mol$^{-1}$ at the CBS limit. With an advanced treatment of correlation effects the dissociation energy further increases as much as 16.1 kcal mol$^{-1}$, reflecting the greater correlation energy of complex **1** compared to its separated constituents. At the FCI-CBS limit the $D_e$ of isomer **1** is determined to be 57.7 ± 0.1 kcal mol$^{-1}$, and the zero-point dissociation energy ($D_0$) is predicted to be 50.9 ± 0.1 kcal mol$^{-1}$.

**Dissociation Energy for Structure 2.** The energy for the structurally straightforward fragmentation of isomer **2**

$$H_6^+(C_s) \rightarrow H_3^+ + H_2 + H \quad (23)$$

based on the FPA is given in Table 12. At the HF level of theory the $D_e$ is determined to be 7.0 kcal mol$^{-1}$ at the CBS limit. With inclusion of correlation effects the $D_e$ inevitably increases, by as much as 5.4 kcal mol$^{-1}$. At the FCI-CBS limit the $D_e$ of isomer **2** is predicted to be 12.4 ± 0.1 kcal mol$^{-1}$, compare with the $D_0$ value 8.3 ± 0.1 kcal mol$^{-1}$.

In this regard, the equilibrium dissociation energies for the following two dissociation reactions

$$H_5^+(C_{2v}) \rightarrow H_3^+ + H_2 \quad (24)$$

and

$$H_6^+(C_s) \rightarrow H_5^+ + H \quad (25)$$

are predicted to be $D_e$ = 9.2 ± 0.1 and 3.1 ± 0.1 kcal mol$^{-1}$, and $D_0$ = 6.4 ± 0.1 and 1.8 ± 0.1 kcal mol$^{-1}$, consistent with the $D_0$ value of $H_5^+$ by Spirko, Amano, Kraemer.[68] It is clearly seen that the complexation energy between $H_3^+$ and $H_2$ in eq 24 is almost three times stronger than that between $H_5^+$ and H in eq 25. This is consistent with the higher frequency of the $H_2\cdots H_3^+$ stretching mode [$\omega_6(a') = 543$ cm$^{-1}$] relative to the $H\cdots H_3^+$ stretching mode [$\omega_7(a') = 408$ cm$^{-1}$] for isomer **2** (in Table 2). By comparison of the results in Tables 11 and 12, the dissociation energy of **1** (in $D_{2d}$ symmetry) is seen to be over 42 kcal mol$^{-1}$ higher than the corresponding value for **2** (in $C_s$ symmetry).

## Concluding Remarks

Ab initio molecular electronic structure theory has been employed in order to systematically investigate six stationary points of the $H_6^+$ hydrogen cluster cation. Full geometrical optimizations have been carried out using highly correlated CCSD, CCSD(T), and CCSDT wave functions and a variety of correlation-consistent cc-pVXZ and aug-cc-pVXZ (where X = D, T, Q) basis sets. Three equilibrium structures (minima, **1**−**3**) and three transition states (first-order saddle points, **4**−**6**) for isomerization reactions have been located. CCSD, CCSD(T), CCSDTQ, and Full CI methods have been used with basis sets as large as sextuple zeta to establish critical energy differences. The $H_2^+$-core cluster with $D_{2d}$ symmetry has been confirmed to be the global minimum on the $H_6^+$ PES. After extensive focal point analyses the following energetics have been deduced: (1) the relative energies of the six structure are summarized in Table

13; (2) the global minimum (the $H_2^+$-core cluster, isomer **1**) lies 3.9 (4.2) ± 0.1 kcal mol$^{-1}$ below the second-lowest minimum (the $H_3^+$-core cluster, isomer **2**), with the ZPVE correction in parentheses; (3) the quartet state isomer **3** with $D_{3h}$ symmetry lies 113.1 (106.9) ± 0.1 kcal mol$^{-1}$ above isomer **1**; (4) the energy barrier for the most important isomerization reaction (**1** → **2**) is 7.4 (5.2) ± 0.1 kcal mol$^{-1}$; (5) the dissociation energy for the global minimum **1** [$H_6^+$ ($D_{2d}$) → $2H_2 + H_2^+$] is 57.5 (50.9) ± 0.1 kcal mol$^{-1}$; (6) the dissociation energy for isomer **2** [$H_6^+$ ($C_s$) → $H_3^+ + H_2 + H$] is 12.3 (8.3) ± 0.1 kcal mol$^{-1}$; and (7) given the low energy of structure **4**, the equilibrium structure **1** is expected to be highly fluxional.

**Acknowledgment.** Q.H. thanks the support by the China Scholarship Council (File No. 2008604057) and the University of Georgia Center for Computational Quantum Chemistry for hospitality during his one year visit. We thank Mr. Tongxiang Lu, Ms. Qunyan Wu, Dr. Francesco A. Evangelista, and Dr. Justin M. Turney for many helpful discussions. This research was supported by National Natural Science Foundation of China (No. 20773016) and the U.S. Department of Energy, Office of Basic Energy Sciences, Grant No. DE-FG02-00ER14748.

## References and Notes

(1) Thomson, J. J. *Philos. Mag.* **1912**, *24*, 209.
(2) Pfeiffer, G. V.; Huff, N. T.; Greenawalt, E. M.; Ellison, F. O. *J. Chem. Phys.* **1967**, *46*, 821.
(3) Poshusta, R. D.; Matsen, F. A. *J. Chem. Phys.* **1967**, *47*, 4795.
(4) Buchheit, K.; Henkes, W. Z. *Angew. Phys.* **1968**, *24*, 191.
(5) Clampitt, R.; Gowland, L. *Nature* **1969**, *223*, 815.
(6) van Deursen, A.; Reuss, J. *Int. J. Mass Spectrom. Ion Phys.* **1973**, *11*, 483.
(7) van Lumig, A.; Reuss, J. *Int. J. Mass Spectrom. Ion Phys.* **1978**, *27*, 197.
(8) Wright, L. R.; Borkman, R. F. *J. Chem. Phys.* **1982**, *77*, 1938.
(9) Kirchner, N. J.; Gilbert, J. R.; Bowers, M. T. *Chem. Phys. Lett.* **1984**, *106*, 7.
(10) Montgomery, J. A.; Michels, H. H. *J. Chem. Phys.* **1987**, *87*, 771.
(11) Kirchner, N. J.; Bowers, M. T. *J. Chem. Phys.* **1987**, *86*, 1301.
(12) Kirchner, N. J.; Bowers, M. T. *J. Phys. Chem.* **1987**, *91*, 2573.
(13) Paul, W.; Schlemmer, S.; Lucke, B.; Gerlich, D. *Chem. Phys.* **1996**, *209*, 265.
(14) Štich, I.; Marx, D.; Parrinello, M.; Terakura, K. *Phys. Rev. Lett.* **1997**, *78*, 3669.
(15) Štich, I.; Marx, D.; Parrinello, M.; Terakura, K. *J. Chem. Phys.* **1997**, *107*, 9482.
(16) Kurosaki, Y.; Takayanagi, T. *J. Chem. Phys.* **1998**, *109*, 4327.
(17) Kurosaki, Y.; Takayanagi, T. *Chem. Phys. Lett.* **1998**, *293*, 59.
(18) Suter, H. U.; Engels, B.; Lunell, S. *Adv. Quantum Chem.* **2001**, *40*, 133.
(19) Kumada, T.; Tachikawa, H.; Takayanagi, T. *Phys. Chem. Chem. Phys.* **2005**, *7*, 776.
(20) Kumada, T.; Takayanagi, T.; Kumagai, J. *J. Mol. Struct.* **2006**, *786*, 130.
(21) Kumagai, J.; Inagaki, H.; Kariya, S.; Ushida, T.; Shimizu, Y.; Kumada, T. *J. Chem. Phys.* **2007**, *127*, 024505.
(22) Kakizaki, A.; Takayanagi, T.; Shiga, M. *Chem. Phys. Lett.* **2007**, *449*, 28.
(23) Shimizu, Y.; Kumada, T.; Kumagai, J. *J. Magn. Reson.* **2008**, *194*, 76.
(24) Jaksch, S.; Mauracher, A.; Bacher, A.; Denifl, S.; da Silva, F. F.; Schöbel, H.; Echt, O.; Märk, T. D.; Probst, M.; Bohme, D. K.; Scheier, P. *J. Chem. Phys.* **2008**, *129*, 224306.
(25) Kurosaki, Y.; Shimizu, Y.; Kumagai, J. *Chem. Phys. Lett.* **2008**, *455*, 59.
(26) Dunning, T. H. *J. Chem. Phys.* **1989**, *90*, 1007.
(27) Kendall, R. A.; Dunning, T. H.; Harrison, R. J. *J. Chem. Phys.* **1992**, *96*, 6796.
(28) Peterson, K. A.; Woon, D. E.; Dunning, T. H. *J. Chem. Phys.* **1994**, *100*, 7410.
(29) Čižek, J. *J. Chem. Phys.* **1966**, *45*, 4256.
(30) Bartlett, R. J. *Annu. Rev. Phys. Chem.* **1981**, *32*, 359.
(31) Bartlett, R. J. *J. Phys. Chem.* **1989**, *93*, 1697.
(32) Purvis, G. D.; Bartlett, R. J. *J. Chem. Phys.* **1982**, *76*, 1910.
(33) Scuseria, G. E.; Scheiner, A. C.; Lee, T. J.; Rice, J. E.; Schaefer, H. F. *J. Chem. Phys.* **1987**, *86*, 2881.
(34) Rittby, M.; Bartlett, R. J. *J. Phys. Chem.* **1988**, *92*, 3033.
(35) Gauss, J.; Lauderdale, W. J.; Stanton, J. F.; Watts, J. D.; Bartlett, R. J. *Chem. Phys. Lett.* **1991**, *182*, 207.
(36) Raghavachari, K.; Trucks, G. W.; Pople, J. A.; Head-Gordon, M. *Chem. Phys. Lett.* **1989**, *157*, 479.
(37) Bartlett, R. J.; Watts, J. D.; Kucharski, S. A.; Noga, J. *Chem. Phys. Lett.* **1990**, *165*, 513.
(38) Watts, J. D.; Gauss, J.; Bartlett, R. J. *Chem. Phys. Lett.* **1992**, *200*, 1.
(39) Watts, J. D.; Gauss, J.; Bartlett, R. J. *J. Chem. Phys.* **1993**, *98*, 8718.
(40) Stanton, J. F. *Chem. Phys. Lett.* **1997**, *281*, 130.
(41) Noga, J.; Bartlett, R. J. *J. Chem. Phys.* **1987**, *86*, 7041.
(42) Scuseria, G. E.; Schaefer, H. F. *Chem. Phys. Lett.* **1988**, *152*, 382.
(43) Watts, J. D.; Bartlett, R. J. *J. Chem. Phys.* **1990**, *93*, 6104.
(44) Werner, H.-J.; Knowles, P. J. *J. Chem. Phys.* **1985**, *82*, 5053.
(45) Knowles, P. J.; Werner, H.-J. *Chem. Phys. Lett.* **1985**, *115*, 259.
(46) Werner, H.-J.; Knowles, P. J. *J. Chem. Phys.* **1988**, *89*, 5803.
(47) Knowles, P. J.; Werner, H.-J. *Chem. Phys. Lett.* **1988**, *145*, 514.
(48) Handy, N. C.; Yamaguchi, Y.; Schaefer, H. F. *J. Chem. Phys.* **1986**, *84*, 4481.
(49) East, A. L. L.; Allen, W. D. *J. Chem. Phys.* **1993**, *99*, 4638.
(50) Császár, A. G.; Allen, W. D.; Schaefer, H. F. *J. Chem. Phys.* **1998**, *108*, 9751.
(51) Gonzales, J. M.; Pak, C.; Cox, R. S.; Allen, W. D.; Schaefer, H. F.; Császár, A. G.; Tarczay, G. *Chem.—Eur. J.* **2003**, *9*, 2173.
(52) Kenny, J. P.; Allen, W. D.; Schaefer, H. F. *J. Chem. Phys.* **2003**, *118*, 7353.
(53) Schuurman, M. S.; Muir, S. R.; Allen, W. D.; Schaefer, H. F. *J. Chem. Phys.* **2004**, *120*, 11586.
(54) Oliphant, N.; Adamowicz, L. *J. Chem. Phys.* **1991**, *95*, 6645.
(55) Kucharski, S. A.; Bartlett, R. J. *J. Chem. Phys.* **1992**, *97*, 4282.
(56) Knowles, P. J.; Handy, N. C. *Chem. Phys. Lett.* **1984**, *111*, 315.
(57) Feller, D. *J. Chem. Phys.* **1993**, *98*, 7059.
(58) Helgaker, T.; Klopper, W.; Koch, H.; Noga, J. *J. Chem. Phys.* **1997**, *106*, 9639.
(59) Gauss, J.; Stanton, J. F.; Bartlett, R. J. *J. Chem. Phys.* **1991**, *95*, 2623.
(60) Gauss, J.; Stanton, J. F. *Chem. Phys. Lett.* **1997**, *276*, 70.
(61) Gauss, J. *J. Chem. Phys.* **2002**, *116*, 4773.
(62) Stanton, J. F.; Gauss, J.; Watts, J. D.; Szalay, P. G.; Bartlett, R. J. With contributions fromAuer, A. A.; Bernholdt, D. E.; Christiansen, O.; Harding, M. E.; Heckert, M.; Heun, O.; Huber, C.; Jonsson, D.; Jusélius, J.; Lauderdale, W. J.; Metzroth, T.; Michauk, C.; O'Neill, D. P.; Price, D. R.; Ruud, K.; Schiffmann, F.; Tajti, A.; Varner, M. E.; Vázquez, J.; and the integral packages: MOLECULE (Almlöf, J.; Taylor, P. R.), PROPS (Taylor, P. R.), and ABACUS (Helgaker, T.; Jensen, H. J. Aa.; Jørgensen, P.; Olsen, J.). Current version see http://www.aces2.de.
(63) Stanton, J. F.; Gauss, J.; Watts, J. D.; Lauderdale, W. J.; Bartlett, R. J. *Int. J. Quantum Chem.* **1992**, *44* (S26), 879.
(64) Werner, H.-J. *MOLPRO, version 2006. 1, a package of ab initio programs.* See: http://www.molpro.net.
(65) Crawford, T. D.; Sherrill, C. D.; Valeev, E. F.; Fermann, J. T.; King, R. A.; Leininger, M. L.; Brown, S. T.; Janssen, C. L.; Seidl, E. T.; Kenny, J. P.; Allen, W. D. J. *Comput. Chem.* **2007**, *28*, 1610.
(66) Ioannou, A. G.; Amos, R. D.; Handy, N. C. *Chem. Phys. Lett.* **1996**, *251*, 52.
(67) Valeev, E. F.; Sherrill, C. D. *J. Chem. Phys.* **2003**, *118*, 3921.
(68) Špirko, V.; Amano, T.; Kraemer, W. P. *J. Chem. Phys.* **2006**, *124*, 244303.

JP905928U